Title: **TCTEX1D2 has two distinct functions in sperm flagellum formation in mice; cytoplasmic dynein 2 and inner dynein arm.**

Ryua Harima[1], Kenshiro Hara[1], Kentaro Tanemura[1,2,*]

[1]Laboratory of Animal Reproduction and Development, Graduate School of Agricultural Science, Tohoku University, 468-1 Aramaki-Aoba, Aoba-ku, Sendai, Miyagi 980-8572, Japan; [2]Laboratory of Reproductive Technology (Repro-SOLEIL), Graduate School of Agricultural Science, Tohoku University, 468-1 Aramaki-Aoba, Aoba-ku, Sendai, Miyagi 980-8572, Japan

*** For correspondence:** kentaro.tanemura.e4@tohoku.ac.jp

Competing interest: The authors declare that no competing interests exist.

Abstract

Flagella and cilia are widely conserved motile structures. Mammalian sperm possess flagella, which confer motility to the sperm and, therefore, are essential for fertilization. Large protein complexes called dynein, including cytoplasmic dynein 2 and axonemal dynein, play a role in the formation of cilia and flagella. The function of each dynein complex subunit in sperm flagellum formation is unclear. One such subunit is TCTEX1D2. *Tctex1d2* $^{-/-}$ mice generated in this study showed male infertility because of flagellar dysplasia arising from round spermatids and disruption of the axonemal structure inside the flagella. In contrast, the motile cilia of *Tctex1d2* $^{-/-}$ mice were normal. Co-immunoprecipitation studies showed that TCTEX1D2 interacted with the cytoplasmic dynein 2 component proteins WDR34, WDR60, and DYNLT1 in the testes and that the localization of these proteins was abnormal in *Tctex1d2* $^{-/-}$ mice. Furthermore, TCTEX1D2 also interacted with WDR63 and WDR78, component proteins of the inner dynein arm, which is axonemal dynein. Overall, we revealed that TCTEX1D2 has two distinct functions in mouse sperm flagellum formation the assembly of cytoplasmic dynein 2 and organization of inner dynein arm which is not the case in cilia formation where TCTEX1D2 functions only as cytoplasmic dynein 2.

Introduction

Flagella are widely conserved structures present in a large number of organisms ranging from protists to mammals, and their most distinctive feature is their motility [1,2]. In mammals, the sperm is the only cell with flagella and thereby has motility, which is essential for fertilization [3]. In addition to flagella, mammalian cells also have a similar motile structure called cilia [4]. The flagellar and cilia axonemes have 9+2 microtubule internal structure, consisting of two central microtubules surrounded by nine peripheral microtubules [5-7]. Large protein complexes called dynein, which move along the microtubules, play important roles in the formation of cilia and flagella and maintenance of motility [8-10]. Dynein is composed of different subunits that are classified as heavy, intermediate, light intermediate, and light chain subunits based on their molecular weight [11]. Dynein is divided into cytoplasmic and axonemal dynein, and cytoplasmic dynein is further divided into cytoplasmic dynein 1 and cytoplasmic dynein 2 [12]. Cytoplasmic dynein 2 and axonemal dynein are closely related to cilia and flagella [13-16]. Cytoplasmic dynein 2 primarily plays a role in cilia formation [17,18] and is responsible for retrograde transport as part of the intraflagellar transport (IFT) system within cilia [18-20]. Axonemal dynein is present as part of the axonemal structure, and divided into outer dynein arm and inner dynein arm. Axonemal dynein generates a sliding force that allows the flagella and cilia to acquire motility [15]. The functions of cytoplasmic dynein 2 and axonemal dynein are very different; therefore, most subunits are specific to either cytoplasmic or axonemal dynein [21,22]. However, light chains are an exception to this rule. In *Chlamydomonas* flagella, some light chains are common between cytoplasmic dynein 2 and axonemal dynein [23,24]. This suggests that dynein light chains are involved in many processes about related to flagella, ranging from formation to structural maintenance. In *Chlamydomonas*, dynein light chains contribute to the assembly of the components, structural stability, and motility of the flagella [24].

In mammals, most studies on dynein light chains have focused on somatic cilia, and very few have focused on sperm flagella. Thus, our understanding of the dynein light chains involved in sperm flagellum formation is very poor. Although flagella are widely conserved structures across species, it is not appropriate to apply the findings from other species to mammalian sperm flagella, because there are differences in the formation mechanisms and constituent proteins between species [2,25-27]. The formation mechanism of sperm flagella and cilia is considered to be similar; however, sperm flagella are generally much longer than cilia and have unique structures, such as mitochondrial sheath, outer dense fiber, and fibrous sheath. Furthermore, it has

71 been reported that the functions of proteins related to axoneme formation differ
72 between sperm flagella and cilia [16], suggesting that there are differences in the
73 mechanism of their formation. Therefore, it is important to use mammalian sperm
74 flagella, to understand the function of dynein light chain in mammalian sperm
75 flagella.
76 In the present study, we focused on Tctex1 domain-containing 2 (TCTEX1D2, also
77 known as DYNLT2B) a dynein light chain present in the testes. In mammalian somatic
78 cells, TCTEX1D2 is known as one of the cytoplasmic dynein 2 light chains and is involved
79 in the formation of primary cilia (non-motile cilia) [11,28,29]. Cytoplasmic dynein 2 has
80 seven light chains (DYNLL1, DYNLL2, DYNLT1, DYNLT3, DYNLRB1, DYNLRB2, and TCTEX1D2)
81 [11,21]; however, the precise function of each subunit is unclear. Among the light chains,
82 only TCTEX1D2 is specific to cytoplasmic dynein 2 [11,28,29], whereas the others are also
83 found in cytoplasmic dynein 1 [11]. In addition, DYNLL1 and DYNLL2, DYNLT1 and DYNLT3,
84 and DYNLRB1 and DYNLRB2 are homologous to each other, and the homologs appear to have
85 interchangeable functions [30]. Therefore, TCTEX1D2 is unique and irreplaceable among
86 the light chains of cytoplasmic dynein 2 and is thought to play a critical role in
87 cytoplasmic dynein 2. However, there are no reports on the role of TCTEX1D2 in sperm
88 flagellum formation, and it is yet unknown whether TCTEX1D2 is a component of
89 cytoplasmic dynein 2 in germ cells. Interestingly, *Tctex1d2* mRNA is highly expressed
90 in mouse testes according to NCBI gene (https://www.ncbi.nlm.nih.gov/gene/66061) and
91 is mainly expressed in spermatocytes according to single-cell RNA-seq in mouse testes
92 [31]. Therefore, it is hypothesized that *Tctex1d2* might play a role in sperm flagellum
93 formation. In this study, we aimed to elucidate the function of *Tctex1d2* in sperm
94 flagellum formation.
95 In this study, we created *Tctex1d2*$^{-/-}$ mice to investigate the function of *Tctex1d2*.
96 Male *Tctex1d2*$^{-/-}$ mice were infertile and displayed severe morphological abnormalities
97 in sperm flagella and disorganized distribution of axonemal components. However,
98 there was no effect on the formation of motile cilia; only the formation of sperm
99 flagella was significantly impaired in *Tctex1d2*$^{-/-}$ mice. TCTEX1D2 interacted with
100 cytoplasmic dynein 2 component proteins in the testes, and we observed that the
101 assembly of the cytoplasmic dynein 2 subunit is blocked in *Tctex1d2*$^{-/-}$ mice. TCTEX1D2
102 also interacted with the subunits of axonemal dynein in the testes. This study revealed
103 that TCTEX1D2 has two distinct functions cytoplasmic dynein 2 and axonemal dynein
104 and plays an important role in sperm flagellum formation in mice.
105

Results

TCTEX1D2 is highly expressed in the testes and localized in flagella from round spermatids to elongated spermatids

Tctex1d2 mRNA is highly expressed in mouse testes according to NCBI gene (https://www.ncbi.nlm.nih.gov/gene/66061). Western blotting (WB) was performed to investigate TCTEX1D2 protein expression. TCTEX1D2 was found to be highly expressed in the testes and spleen (fig. 1A). This shows that TCTEX1D2 may have certain functions in the testes. To determine the localization of TCTEX1D2 in germ cells, we performed immunohistochemistry (IHC) and immunocytochemistry (ICC) experiments. However, no antibodies were available for the IHC or ICC analyses. Therefore, we generated *Tctex1d2* - 3×FLAG mice, in which a 3×FLAG was knocked in at the N-terminus of *Tctex1d2* (fig. S1A) and implemented ICC in germ cells isolated from the testes of these mice. Spermatogenesis in *Tctex1d2* - 3×FLAG mice was comparable to that in WT mice, and the sperm flagella of *Tctex1d2* - 3×FLAG mice showed normal morphology (fig. S1B, C). Thus, 3×FLAG knock-in in *Tctex1d2* had no effect on the function of TCTEX1D2. We found that TCTEX1D2 was localized along the flagella from round spermatids to elongated spermatids. (fig. 1B-D). TCTEX1D2 was also localized in the manchette, which are transiently formed in step 10-14 spermatids (fig. 1C). Furthermore, TCTEX1D2 was also expressed in the cilia of ventricles, trachea, and oviducts (fig. S2A-C).

TCTEX1D2 is a component of cytoplasmic dynein 2

In mammalian somatic cells, TCTEX1D2 is a component of cytoplasmic dynein 2 (fig. 2A). Therefore, we analyzed whether TCTEX1D2 is a component of cytoplasmic dynein 2 in germ cells. Cytoplasmic dynein 2 consists of 11 subunits: heavy chain (DYNC2H1), intermediate chain (WDR34 and WDR60), light intermediate chain (DYNC2LI1), and light chain (DYNLRB1, DYNLRB2, DYNLL1, DYNLL2, DYNLT1, DYNLT3, and TCTEX1D2) (fig. 2A). In mammalian somatic cells, TCTEX1D2 interacts with DYNLT1 and WDR60 [30]. In the testes, TCTEX1D2 interacted not only with WDR60 and DYNLT1, but also with WDR34 (fig. 2B). These results indicate that TCTEX1D2 is one of the components of cytoplasmic dynein 2 in germ cells.

TCTEX1D2 is an axoneme component and interacts with subunits of the inner dynein arm

In the flagella of *Chlamydomonas*, Tctex2b (a homolog of mouse TCTEX1D2) is present as a light chain of the inner dynein arm in the axoneme dynein [32]. The inner dynein arm is important for controlling the size and shape of the bend of the flagella, features collectively referred to as waveforms [33]. In *Chlamydomonas*, loss of function

142 of the inner arm dynein subunit causes impaired flagellar motility [34-36]. Thus, it is
143 believed that in mammals, TCTEX1D2 is present in the sperm flagella as a light chain
144 of the inner dynein arm. We analyzed the protein expression of TCTEX1D2 in the
145 spermatozoa of the cauda epididymis. WB analysis of sperm proteins fractionated into
146 Triton X-100 soluble, SDS soluble, and SDS-insoluble fractions was performed. SLC2A3,
147 Ac-α-tubulin, and AKAP3 are markers for sperm membrane, axoneme, and other insoluble
148 fractions, respectively. TCTEX1D2 was present in both the SDS-soluble and
149 SDS-resistant fractions (fig. 2C). ICC studies also revealed that TCTEX1D2 localized
150 along the sperm flagella (fig. 2D). These results showed that TCTEX1D2 is an axoneme
151 component in mice. Further, co-immunoprecipitation studies revealed that TCTEX1D2
152 interacted with WDR63 and WDR78 (fig. 2E). Both proteins are intermediate chains of
153 the inner dynein arm, which is a component of the 9+2 microtubule structure. These
154 results indicate that TCTEX1D2 has some functions in the light chain of the inner
155 dynein arm in mouse sperm flagella, as well as in that of *Chlamydomonas* flagella.
156
157 ***Tctex1d2* is essential for male fertility**
158 To explore the function of TCTEX1D2 in the mouse testes, we generated *Tctex1d2*
159 knockout (*Tctex1d2* $^{-/-}$) mice using the CRISPR/Cas9 system (fig. 3A). We confirmed a
160 4696-bp deletion in the generated knockout mice using genotyping and Sanger sequencing
161 (fig. 3B, C). Furthermore, the generated knockout mice completely lost TCTEX1D2
162 protein expression, as shown by results of WB experiments (fig. 3D). Fertility tests
163 were conducted to assess the fertility of *Tctex1d2* $^{-/-}$ male mice. *Tctex1d2* $^{-/-}$ male mice
164 were mated with two wild-type (WT) female mice. *Tctex1d2* $^{-/-}$ male mice were found to
165 be completely infertile (fig. 3E). In contrast, the testis/body weight ratio was
166 unchanged in *Tctex1d2* $^{-/-}$ mice in comparison with *Tctex1d2* $^{+/+}$ mice (fig. 3F).
167
168 ***Tctex1d2* $^{-/-}$ mice exhibit abnormal morphology of sperm flagella, but not of cilia**
169 To identify the cause of infertility in *Tctex1d2* $^{-/-}$ male mice, we performed
170 periodic acid-Schiff hematoxylin (PAS-H) staining of the testes and epididymis. In
171 stage I-III seminiferous tubules, a layered structure of germ cells was observed (fig.
172 4A, yellow box) and numerous spermatid flagella were present in the tubule lumen of
173 *Tctex1d2* $^{+/+}$ mice (fig. 4A, red box arrow). In contrast, a layered structure of germ
174 cells was observed (fig. 4B, yellow box), but only a few flagella were present in
175 the tubule lumen of *Tctex1d2* $^{-/-}$ mice (fig. 4B, red box). In stage Ⅶ seminiferous
176 tubules, a large number of elongated spermatids were observed in the lumen in *Tctex1d2*
177 $^{+/+}$ mice (fig. 4C). However, only a few elongated spermatids were observed in the lumen

178 of *Tctex1d2* $^{-/-}$ mice (fig. 4D), and the number of spermatozoa was significantly
179 decreased in the cauda epididymis (fig. 4E, F). Furthermore, almost all the sperm
180 flagella of *Tctex1d2* $^{-/-}$ mice showed markedly abnormal morphology compared with those
181 of *Tctex1d2* $^{+/+}$ mice (fig. 4G), such as shortened and coiled tails (fig. 4H). In mice,
182 the epithelial cells of the ventricles, trachea, and oviducts have motile cilia
183 similar to sperm flagella. We analyzed the morphology of these cilia using Hematoxylin
184 -Eosin (HE) staining. In contrast to the severe defects in sperm flagella, the cilia
185 of the ventricles, trachea, and oviducts showed no abnormal morphology in *Tctex1d2*
186 $^{-/-}$ mice (fig. S3A-C). Therefore, we concluded that only the sperm flagella showed
187 severely abnormal morphology in *Tctex1d2* $^{-/-}$ mice.
188
189 **_Tctex1d2_ $^{-/-}$ mice show abnormal sperm flagella and disruption of axoneme structures**
190 **in early round spermatids**
191 The results shown in fig. 1B-D indicate that TCTEX1D2 is expressed from the early
192 stage of sperm flagellum formation and may have some functions at that stage. To
193 further understand the role of TCTEX1D2, we analyzed flagellum formation during
194 spermiogenesis. Flagellum formation in *Tctex1d2* $^{-/-}$ mice was normal until steps 2-3
195 of the spermatids (fig. 5A). However, the axoneme failed to elongate normally and
196 showed significant defects from step 4 spermatids onwards in *Tctex1d2* $^{-/-}$ mice (fig.
197 5A). Using transmission electron microscopy, we examined the internal structure of
198 the flagella and found that the axonemal components were disorganized in *Tctex1d2*
199 $^{-/-}$ mice. Doublet microtubules were not formed and many single microtubules were
200 observed in *Tctex1d2* $^{-/-}$ mice (fig. 5B). Moreover, the 9＋2 microtubule structure, inner
201 dynein arm (IDA), outer dynein arm (ODA), outer dense fiber (ODF), and fibrous sheath
202 (FS) were disorganized and scattered in *Tctex1d2* $^{-/-}$ mice (fig. 5B). Thus, the cause
203 of the failure of flagellar elongation in *Tctex1d2* $^{-/-}$ mice was disruption of the
204 axonemal structure. These results suggested that TCTEX1D2 plays an important role
205 in the organization of axonemal components.
206
207 **TCTEX1D2 functions in the assembly of cytoplasmic dynein 2 subunits**
208 TCTEX1D2 is one of the components of cytoplasmic dynein 2 in germ cells. Therefore,
209 we investigated the expression patterns of TCTEX1D2 interacted subunit (WDR60, WDR34,
210 and DYNLT1) in *Tctex1d2* $^{-/-}$ mice using ICC. WDR60 and WDR34 were not expressed in the
211 flagella both *Tctex1d2* $^{+/+}$ and *Tctex1d2* $^{-/-}$ mice round spermatids (fig. 6A, B). In the
212 flagella in *Tctex1d2* $^{+/+}$ mice elongated spermatids, WDR60 localized along the flagellar,
213 especially strongly in principal piece (fig. 6A). WDR34 also localized along the

214 flagellar, especially strongly in middle piece (fig. 6B). However, expression
215 patterns of WDR60 and WDR34 were abnormal in *Tctex1d2* $^{-/-}$ mice elongated spermatids,
216 including loss of signal (fig. 6A, B above) and ectopic signal (fig, 6A, B bellow
217 arrow head). DYNLT1 uniformly localized along the flagellar in *Tctex1d2* $^{+/+}$ mice round
218 spermatids to elongated spermatids (fig. 6C). However, in *Tctex1d2* $^{-/-}$ mice, expression
219 of DYNLT1 decreased in the flagella of round spermatids and loss in elongated
220 spermatids (fig. 6C). These results suggest that TCTEX1D2 plays a role in the assembly
221 and structural stability of the cytoplasmic dynein 2 subunits.
222 During flagellum formation, the components that constitute the flagella are
223 transported along microtubules. The IFT system is responsible for this transport and
224 consists mainly of IFT proteins, kinesin 2, cytoplasmic dynein 2, and the BBSome
225 complex [9,37-39]. As *Tctex1d2* $^{-/-}$ mice showed abnormal cytoplasmic dynein 2 localization,
226 we analyzed the expression patterns of other IFT systems. IFT88, an IFT protein, and
227 DYNC2LI1 showed decreased signals and ectopic expression in the flagella of elongated
228 spermatids in *Tctex1d2* $^{-/-}$ mice (fig, S4A, B). In contrast, IFT140 (an IFT protein),
229 KIF3A (a component of kinesin 2), and DYNC2H1 were localized normally in the flagella
230 of elongated spermatids in *Tctex1d2* $^{-/-}$ mice (fig. S4C~E). These results suggest that
231 the IFT system is partially defective in *Tctex1d2* $^{-/-}$ mice. These results are
232 represented in the schematic diagram (fig. 6D). In *Tctex1d2* $^{+/+}$ mice elongated
233 spermatids, the 11 subunits of cytoplasmic dynein 2 form complexes and move on
234 microtubules (fig. 6D). However, *Tctex1d2* $^{-/-}$ mice elongated spermatids, DYNC2LI1,
235 WDR60, WDR34 and DYNLT1 among the 11 subunits showed abnormal localization and were
236 not assembled in the cytoplasmic dynein 2 complex (fig. 6D). Therefore, TCTEX1D2 plays
237 a role in the assembly of cytoplasmic dynein 2 subunits.
238

239 ## Discussion

240 In this study, we identified TCTEX1D2 as a dynein light chain important for sperm
241 flagellum formation in mice. *Tctex1d2* $^{-/-}$ mice showed abnormal flagella in round
242 spermatids and disorganization of axonemal components in the flagella. TCTEX1D2 was
243 identified as a component of cytoplasmic dynein 2, based on its interaction with WDR34,
244 WDR60, and DYNLT1, and the expression patterns of these proteins was found to be
245 aberrant in the elongated spermatids of *Tctex1d2* $^{-/-}$ mice. In addition, IFT88 and
246 DYNC2LI1 showed similar abnormal expression patterns in the elongated spermatids of
247 *Tctex1d2* $^{-/-}$ mice. These results suggested that the assembly of cytoplasmic dynein 2
248 was impaired in *Tctex1d2* $^{-/-}$ mice, consequently affecting the stability of the IFT
249 system. Cilia formation is impaired when the functions of the cytoplasmic dynein 2
250 and IFT proteins are completely lost [40-43]. However, the formation of primary cilia
251 is normal in TCTEX1D2 knockout somatic cells in mammalian [30], and the formation of
252 motile cilia was normal in *Tctex1d2* $^{-/-}$ mice generated in this study. The expression
253 patterns of cytoplasmic dynein 2, kinesin 2, and IFT proteins were normal in *Tctex1d2*
254 $^{-/-}$ mice (fig. S5A-C). Therefore, the loss of TCTEX1D2 had no significant effect on
255 the IFT system, and cytoplasmic dynein 2 and IFT proteins functioned normally in the
256 sperm flagella and cilia of *Tctex1d2* $^{-/-}$ mice. Indeed, as some components of the IFT
257 system, such as KIF3A, DYNC2H1, and IFT140, are expressed normally in the flagella
258 of *Tctex1d2* $^{-/-}$ mice, it can be concluded that the IFT system works properly during
259 sperm flagellum and cilia formation in *Tctex1d2* $^{-/-}$ mice. Moreover, TCTEX1D2 was
260 expressed in the flagella of round spermatids, and *Tctex1d2* $^{-/-}$ mice showed abnormal
261 flagella in early round spermatids, whereas WDR34 and WDR60 were not expressed in
262 the flagella of round spermatids. As flagellar abnormalities in *Tctex1d2* $^{-/-}$ mice
263 occurred before WDR34 and WDR60 expression, TCTEX1D2 has some functions prior to its
264 function as cytoplasmic dynein 2. Considering these points, the impairment in
265 cytoplasmic dynein 2 by *Tctex1d2* deficit has only a minor effect on sperm flagellum
266 formation therefore, it should be other major causes the flagellar disorders seen
267 in *Tctex1d2* $^{-/-}$ mice.

268 Another explanation is that TCTEX1D2 functions as an axonemal structure. In
269 *Chlamydomonas*, Tctex2b (a homolog of mouse TCTEX1D2) is present in the axoneme as
270 the light chain of the inner dynein arm [32,44]. In the present study, we found that
271 TCTEX1D2 was localized in the sperm axoneme and interacted with WDR63 and WDR78. Thus,
272 it was confirmed that TCTEX1D2 is present in the axoneme as a light chain of the inner
273 dynein arm. Transmission electron microscopy revealed that the inner dynein arm was
274 aberrant in the axoneme of the sperm of *Tctex1d2* $^{-/-}$ mice. These results indicate that

275 TCTEX1D2 is important for inner dynein arm assembly. In a previous study, it was shown
276 that *Wdr63* knockout mice exhibited deficiency of sperm flagella and a disruption of
277 the axoneme structure similar to what was seen in *Tctex1d2* $^{-/-}$ mice [45]. Disorganization
278 and structural instability of the inner dynein arm causes sperm flagellar dysplasia.
279 Therefore, flagellar disorders observed in *Tctex1d2* $^{-/-}$ mice are mainly owing to defects
280 in the inner dynein arm. We intended to perform ICC studies using anti-WDR63 and
281 anti-WDR78 antibodies in *Tctex1d2* $^{-/-}$ mice. However, we could not confirm whether the
282 loss of TCTEX1D2 affects the dynamics of WDR63 and WDR78.
283 Despite *Tctex1d2* $^{-/-}$ mice having a severely phenotype in sperm flagella, there were
284 no defects in the cilia of the ventricle, trachea, and oviduct. This difference is
285 likely owing to the fact that TCTEX1D2 expressed in the cilia of the ventricles,
286 trachea and oviduct functions only as cytoplasmic dynein 2, not as inner dynein arm,
287 thus weakening the effects of TCTEX1D2 deficit. In a previous study, it was shown
288 that the axonemal components and proteins necessary for axoneme formation differed
289 between sperm flagella and cilia [16]. Therefore, the function of TCTEX1D2 as an inner
290 dynein arm is unique to sperm flagella. On the other hand, sperm flagella were not
291 completely absent in *Tctex1d2* $^{-/-}$ mice, normally formed up to a certain length in the
292 steps 2-3 round spermatids. As flagella are characterized by a much greater length
293 than cilia, flagellum formation may be undergone a specific change to retain TCTEX1D2
294 inside the axonemes to maintain the length of flagella. A phenotype similar to that
295 observed in the sperm of *Tctex1d2* $^{-/-}$ mice was observed with CFAP61 deletion. CFAP61,
296 which is a conserved component of the calmodulin- and radial spoke-associated complex
297 of cilia and flagella [46,47], when deleted in mice, resulted in motile cilia of normal
298 length; however, the sperm flagella failed to maintain their length [47]. Furthermore,
299 some knockout mice with axonemal components show normal formation of motile cilia
300 but severe defects in sperm flagella [16]. Therefore, despite the sperm flagella being
301 regarded as having a structure similar to that of motile cilia, unique molecular
302 mechanisms give rise to the characteristic length and internal structure during its
303 formation.
304 In the dynein light chain related to cilia and flagella formation, *Tctex1d2* was
305 the first gene to be identified as leading to severe defects in sperm flagella when
306 knocked out in mice. This study showed that dynein light chains, like other chains,
307 play an essential role in sperm flagellum formation in mammals. During cilia formation
308 in mammalian somatic cells, it is known that TCTEX1D2 functions as cytoplasmic dynein
309 2 [11,18]. However, during sperm flagellum formation, TCTEX1D2 functions as an inner
310 dynein arm in addition to its function as cytoplasmic dynein 2. Thus, dynein light

311 chains are involved in many processes related to sperm flagella from formation to
312 structural maintenance in mammals. *Tctex1d2* $^{-/-}$ mice showed defective sperm flagella,
313 whereas the Tctex2b mutant *Chlamydomonas* did not show defective flagella but only
314 reduced motility [32,44]. This indicates that the function of homologous genes differs
315 among species, and it is important to analyze each species.
316 Multiple morphological abnormalities of the sperm flagella (MMAF) is a male
317 infertility with genetic component, one of the most severe form of sperm defect [48].
318 MMAF is characterized abnormal flagella, including short, coiled, absent and of
319 irregular caliber flagellar [49]. A number of genes have been identified to be associated
320 with MMAF [50], yet only 35-60% of MMAF cases have been identified and need for further
321 study to discover new MMAF-related genes [51,52]. The phenotype of *Tctex1d2* $^{-/-}$ mice is
322 similar to cases seen in MMAF, suggesting that Tctex1d2 deficiency may cause MMAF
323 in human. WDR63, which interacted with TCTEX1D2, is an MMAF-related gene and biallelic
324 variants in WDR63 were identified in infertility men [45]. Therefore, it is possible
325 that TCTEX1D2 is also a candidate gene causing MMAF. Our study leads to uncover the
326 new MMAF causative genes and could be used as a genetic diagnostic indicator for male
327 infertility.
328 In summary, we identified *Tctex1d2* as a novel gene essential for the formation
329 of mouse sperm flagella. *Tctex1d2* $^{-/-}$ mice exhibited a severely phenotype only in the
330 sperm flagella, whereas motile cilia had normal structure and function. TCTEX1D2 is
331 weakly involved in the assembly of cytoplasmic dynein 2 and IFT proteins and is
332 important for the assembly and structural stability of the inner dynein arm; this
333 function is unique to sperm flagellum formation, and is not a part of cilia formation.
334 These findings provide novel insights into the function of the dynein light chain
335 in sperm flagellum formation and contribute to the elucidation of the differences
336 between the formation mechanism of sperm flagella and cilia.
337
338

339 ## Materials and Methods

340 ### Animals

341 All mice were C57BL/6N background. C57BL/6N mice were purchased from SLC and
342 maintained under a 12-h light/dark cycle. All animal care and experimental procedures
343 were conducted according to protocols approved by the Tohoku University Institutional
344 Animal Care and Use Committee (2019noudou-003-02, 2019noukumikae-030-06).

345

346 ### Generation of *Tctex1d2* $^{-/-}$ mice and *Tctex1d2* - 3×FLAG mice

347 *Tctex1d2* knockouts of the C57BL/6N strain were generated using *i*-GONAD as previously
348 reported [53]. Briefly, crRNA was designed with the following sequences:
349 5'-GGTTTGAACCACTACGGTGT-3' and 5'-TATTCAAGAACTAAGCCCTC-3'. In addition, crRNA
350 and tracrRNA (Integrated DNA Technologies) were annealed at 94°C for 2 min, mixed
351 with Cas9 nuclease, and injected into the oviduct at E0.7 of plug confirmed mice.
352 Primer sequences for genotyping are given below.
353 Fw1:5'-ATGCGTGCAAGGATGAGCTA-3', Rv1:5'-AGGATTTGATCCCCAGCGTG-3', and Rv2:
354 GCTGGACAACCAGGAAGTGT.
355 The PCR product from the mutant gDNA was sequenced by Sanger sequencing to confirm
356 successful deletion. To fix the mutation in the strain, the F0 founder was mated with
357 wild-type (WT) mice, and the resulting F1 heterozygous male and female mice were
358 crossed to obtain an F2 generation containing homozygous mutants. The established
359 strain was maintained by sibling breeding and used in the current study.
360 The method for the generating *Tctex1d2* - 3×FLAG mice was the same as described above.
361 crRNA was designed with the following sequence: 5'-TTGGACCAGACGCAGGGATA-3'. ssODN
362 was designed with the following sequence:
363 5'-GAGCCGCAACCGACCACACTTCCTTCTAGAGATCTGTTGGACCAGCCGCTGAGCTATGGACTACAAGGACCACGAC
364 GGCGATTATAAGGATCACGACATCGACTACAAAGACGACGATGACAAGGCTGTGTCCTTCCGCGGCCTGTCCTTATCGGC
365 TCACTCCGAGGGCTTGAGTGAGGTCG-3'. crRNA and tracrRNA (Integrated DNA Technologies)
366 were annealed, mixed with ssODN and Cas9 nuclease, and injected into the oviduct.

367

368 ### Fertility test

369 A single 12-week-old male mouse (*Tctex1d2* $^{+/+}$ or *Tctex1d2* $^{-/-}$) was caged with two
370 8-week-old female WT mice for 4 weeks. Mating was verified by monitoring the presence
371 of vaginal plugs. The plugged females were then replaced with fresh mice. Litter size
372 was scored for the females that had plugs.

373

374 ### Histological analysis

375 Mice were euthanasia, and the testes, epididymis, brain, trachea, and oviducts were
376 collected from *Tctex1d2* $^{+/+}$ and *Tctex1d2* $^{-/-}$ mice. Testes and epididymides were fixed
377 in Bouin's solution, whereas brain, trachea, and oviducts were fixed in 4 %
378 paraformaldehyde. The fixed tissues were gradually dehydrated using graded series
379 of ethanol and xylene at different concentrations and finally embedded in paraffin.
380 Sections were rehydrated, the testes and epididymis were stained with periodic
381 acid-Schiff (PAS), and the ventricle, trachea, and oviduct were stained with
382 hematoxylin-eosin and examined under a microscope (Olympus BX50).
383
384 **Immunohistochemistry**
385 Immunohistochemistry (IHC) studies were performed as previously described [54]. Tissue
386 sections were placed in antigen retrieval buffer (pH 6.0; citrate buffer) for 20 min
387 at 90 ℃. The following primary antibodies were used: rabbit anti-DYKDDDDK tag
388 antibody (20543-1-AP, Proteintech), mouse anti-acetylated α tubulin antibody
389 (sc-23950, Santa Cruz), rabbit anti-TCTEX1 antibody (ab202583, Abcam), rabbit
390 anti-IFT88 antibody (13967-1-AP, Proteintech), and rabbit anti-KIF3A (13930-1-AP,
391 Proteintech). The samples were examined under a fluorescence microscope (Keyence
392 BZ-X710).
393
394 **Immunocytochemistry of testicular germ cells**
395 For staining individual cells, samples were prepared using the following protocol.
396 Seminiferous tubules were fixed with 2 % paraformaldehyde containing 0.1 % Triton
397 X-100 for 10 min at room temperature (RT). Pieces of tubules were placed in a drop
398 of the fixing solution on a glass slide, and the pieces were minced in the drop. The
399 slides were gently tapped on the coverslips using tweezers and frozen in liquid
400 nitrogen for 30 s and coverslips were removed. The slides were washed thrice with
401 PBS for 5 min and immunostained. The slides were treated with blocking buffer (Blocking
402 One, Nacalai Tesque, 03953-95) for 1 h at RT and incubated with primary antibody
403 overnight at 4 ℃. The following primary antibodies were used: mouse anti-acetylated
404 α tubulin antibody (sc-23950, Santa Cruz), mouse anti-FLAG M2 antibody (F1804,
405 Sigma-Aldrich), rabbit anti-WDR60 antibody (NBP1-90437, Novus Biologicals), rabbit
406 anti-WDR34 antibody (NBP1-88805, Novus Biologicals), rabbit anti-TCTEX1 antibody
407 (ab202583, Abcam), rabbit anti-DYNC2H1 antibody (MBS7050711, MyBioSource), rabbit
408 anti-DYNC2LI1 antibody (PA5-98717, Thermo Fisher Scientific), rabbit anti-IFT88
409 antibody (13967-1-AP, Proteintech), rabbit anti-KIF3A (13930-1-AP, Proteintech), and
410 rabbit anti-IFT140 antibody (17460-1-AP, Proteintech). Acrosomes were stained with

411 Alexa Fluor 568-conjugated Lectin PNA (L32458; Thermo Fisher Scientific). The samples
412 were examined under a fluorescence microscope (Keyence BZ-X710).
413
414 **Western blotting**
415 The tissues (brain, trachea, lung, heart, liver. spleen, kidney, testis) were lysed
416 using RIPA buffer (Nacalai Tesque, 08714-04) containing 1 % phosphatase inhibitor
417 (Nacalai Tesque, 07575-51), and incubated for 30 min on ice. The lysates were
418 centrifuged at 15,000 × *g* for 15 min at 4 ℃ and eluted with sample buffer for 5
419 min at 100 ℃. The samples were separated by SDS-PAGE, transferred to a PVDF membrane,
420 and treated with a commercial blocking buffer (Blocking One, Nacalai Tesque, 03953-95)
421 for 1 h at RT. The membranes were then incubated with primary antibody overnight at
422 4 ℃. The following primary antibodies were used: rabbit anti-TCTEX1D2 antibody
423 (PA5-116015, Thermo Fisher Scientific) and mouse anti-β-actin antibody (Santa Cruz
424 sc-47778). After washing three times with TBS-T for 5 min, the membranes were
425 incubated with anti-rabbit or anti-mouse HRP-conjugated antibodies (W4011 and W4021,
426 Promega) for 1 h at RT. Images were captured using an ImageQuant LAS 500 (Cytiva).
427
428 **Immunoprecipitation**
429 Testes were lysed using RIPA buffer (Nacalai Tesque, 08714-04), and incubated for
430 30 min on ice. The lysates were centrifuged at 15,000 × *g* for 15 min at 4 ℃ and
431 were incubated for overnight at 4 ℃ with anti-FLAG M2 antibody (F1804,
432 Sigma-Aldrich). Subsequently, the lysates were conjugated with 25 µl Protein G Mag
433 Sepharose™ (28944008, cytiva) for 2 h at 4 ℃. The immune complexes were washed three
434 times with TBS-T for 5 min and eluted with sample buffer for 10 min at 100 ℃. Samples
435 were separated using SDS-PAGE and western blot analysis was subsequently performed.
436 Membranes were stripped with a stripping buffer (Nacalai Tesque, 05364-55), and used
437 for other antibody reactions, as required. The following primary antibodies were used
438 for western blotting: rabbit anti-TCTEX1D2 (PA5-116015, Thermo Fisher Scientific),
439 rabbit anti-WDR60 (NBP1-90437, Novus Biologicals), rabbit anti-WDR34 (NBP1-88805,
440 Novus Biologicals), rabbit anti-TCTEX1 (ab202583, Abcam), mouse anti-WDR78
441 (sc-390633, Santa Cruz Biotechnology), and rabbit anti-WDR63 antibody (NBP2-32639,
442 Novus).
443 Images were captured using the ImageQuant LAS 500 (cytiva).
444
445 **Fractionation of spermatozoa**
446 Cauda epididymis spermatozoa were suspended in 1 % Triton X-100 lysis buffer (50 mM

447 NaCl, 20 mM Tris-HCl, pH 7.5, protease inhibitor mixture) and incubated for 2 h at
448 4 ℃. The sample was centrifuged at 15,000 × *g* for 10 min to separate the
449 Triton-soluble fraction (supernatant) from the Triton-resistant fraction (pellet).
450 The pellet was resuspended in 1 % SDS lysis buffer (75 mM NaCl, 24 mM EDTA, pH 6.0,
451 protease inhibitor mixture) and incubated for 1 h at RT. The sample was centrifuged
452 at 15,000 × *g* for 10 min to separate the SDS-soluble fraction (supernatant) and the
453 SDS-resistant fraction (pellet). The pellet was dissolved in sample buffer for 10
454 min at 100 ℃. Samples were separated using SDS-PAGE and western blot analysis was
455 subsequently performed. The following primary antibodies were used: rabbit
456 anti-DYKDDDDK tag antibody (20543-1-AP, Proteintech), rabbit anti-GLUT3 antibody
457 (20403-1-AP, Proteintech), mouse anti-acetylated α tubulin antibody (sc-23950,
458 Santa Cruz), and rabbit anti-AKAP3 antibody (13907-1-A, Proteintech). The samples
459 were examined under a fluorescence microscope (Keyence BZ-X710).
460
461 **Immunofluorescence for spermatozoa**
462 Cauda epididymis spermatozoa was incubated inhuman tubular fluid (HTF) medium for
463 1 h at 37.5 ℃ with 5 % CO_2, and swim-up spermatozoa was collected and washed with
464 PBS. The suspension was fixed in 4 % paraformaldehyde for 10 min at RT and air dried
465 on slide glass. The slides were permeabilized with 0.2 % Triton X-100 for 10 min at
466 37 ℃ and were washed three times in PBS at 5 min. The slides were treated with blocking
467 buffer (Blocking One, Nacalai Tesque, 03953-95) for 1 h at RT and incubated with
468 primary antibody overnight at 4 ℃. The following primary antibodies were used: rabbit
469 anti-DYKDDDDK tag antibody (20543-1-AP, Proteintech) and mouse anti-acetylated α
470 tubulin antibody (sc-23950, Santa Cruz). The samples were examined under a
471 fluorescence microscope (Keyence BZ-X710).
472
473 **Sperm motility, count, and abnormal sperm ratio analyses**
474 Cauda epididymis sperm was incubated in HTF sodium for 1 h at 37.5 ℃ with 5 % CO_2.
475 Sperm motility parameters were evaluated using a computer-assisted sperm analysis
476 (CASA) system (SMAS；DITECT). Sperm count was analyzed using a hemocytometer. Abnormal
477 sperm ratios were analyzed using phase-contrast microscopy, and 200 sperms from each
478 sample were observed.
479
480 **Transmission electron microscopy**
481 *Tctex1d2*$^{+/+}$ or *Tctex1d2*$^{-/-}$ mice testes were cut into 1-mm-thick sections and were fixed
482 with 2.5 % glutaraldehyde in 0.1 M phosphate buffer (PB) for 1.5 h at RT. After the

483 tissues were washed in PB three times, they were additionally fixed with 1 % OsO_4 in
484 0.1 M PB for 1.5 h at 4 ℃. The tissues were dehydrated using a graded ethanol series
485 for 10 min at RT, which was then replaced with 50 % propylene oxide (PO) in ethanol
486 followed by 100 % PO for 10 min each at RT. The tissues were permeabilized with a
487 mixture of PO and epoxy resin at RT (PO: epoxy resin = 2:1 for 2 h, PO: epoxy resin
488 = 1:1 for 4 h, PO: epoxy resin = 1:2 for 12 h, only epoxy resin for 24 h). The tissues
489 were embedded in epoxy resin for 12 h at 37 ℃, for 12 h at 45 ℃, and for 12 h at
490 60 ℃. Ultrathin sectioning, staining, and imaging were performed at an external lab.
491
492 **Statistical analyses**
493 The unpaired Student's *t*-test (Microsoft Office Excel; Microsoft Corporation) was
494 used for comparisons with *Tctex1d2*$^{+/+}$ mice. Values are represented as the mean ± SE.
495 Differences were considered significant at $p < 0.05$, indicated as $p < 0.05$ (*).
496

497 **Figure legends**

498 Figure. 1. TCTEX1D2 was high expression in the testis and localized along the flagella
499 from round spermatids to elongated spermatids and the manchette. (A) Protein
500 expression analysis of mouse TCTEX1D2 in various organs using western blotting (WB);
501 TCTEX1D2 was highly expressed in the testes and spleen. (B-D) ICC in WT and *Tctex1d2*
502 - 3×FLAG germ cells to analyze the localization of TCTEX1D2 (green: anti-FLAG, red:
503 anti-acetylated-α-tubulin, blue: hoechst33342). TCTEX1D2 localized to flagella from
504 early round spermatids to elongated spermatids. In addition, TCTEX1D2 localized to
505 the manchette. (B) Round spermatids in steps 1-3. (C) Elongated spermatids of steps
506 10-12. (D) Elongated spermatids of steps 15-16. Scale bars are 10 μm.

507

508 Figure. 2. TCTEX1D2 interacted with the subunits of cytoplasmic dynein 2 and axonemal
509 dynein. (A) Schematic diagram of the cytoplasmic dynein 2 complex in somatic cell.
510 (B) Co-immunoprecipitation in the testes of *Tctex1d2* - 3×FLAG mice. In the testes,
511 TCTEX1D2 interacted with WDR60, WDR34, and DYNLT1. (C) WB of cauda epididymis sperm
512 fractionated into Triton X-100 soluble, SDS-soluble, and SDS-insoluble fractions from
513 WT and *Tctex1d2* - 3×FLAG mice. TCTEX1D2 detected in SDS-soluble and SDS-insoluble
514 fractions. (D) ICC of cauda epididymis sperm from WT and *Tctex1d2* - 3×FLAG mice
515 (green: FLAG, red: acetylated-α-tubulin, blue: hoechst33342). TCTEX1D2 localized
516 along the flagella. Asterisks indicate non-specific signals. Scale bars are 10 μm.
517 (E) Co-immunoprecipitation with WDR63 and WDR78 in the testes of *Tctex1d2* - 3×FLAG
518 mice. TCTEX1D2 interacted with WDR63 and WDR78. The used membrane was same as that
519 in (B).

520

521 Figure. 3. TCTEX1D2 was required for male fertility. (A) Schematic representation
522 of the generation of *Tctex1d2* $^{-/-}$ mice. The gRNA was designed between exons 1 and 2
523 and between exons 3 and 4. Genotyping primer pairs were Fw1 and Rv1 for *Tctex1d2* $^{+/+}$
524 mice, Fw1 and Rv2 for *Tctex1d2* $^{-/-}$ mice. (B) Genotyping and (C) Sanger sequencing showed
525 that *Tctex1d2* $^{-/-}$ mice had a 4696 bp deletion within the target region. (D) WB of tissue
526 from mouse testes confirmed that TCTEX1D2 protein expression was completely lost in
527 *Tctex1d2* $^{-/-}$ mice. (E) Male *Tctex1d2* $^{+/+}$ and *Tctex1d2* $^{-/-}$ mice were mated with two female
528 WT mice. We observed 33 plugs in *Tctex1d2* $^{-/-}$ mice; however, *Tctex1d2* $^{-/-}$ mice were unable
529 to sire any offspring. (F) The ratio of testes weight / body weight. There were no
530 differences between *Tctex1d2* $^{+/+}$ and *Tctex1d2* $^{-/-}$ mice. Error bars indicate means ±
531 S.E. Two-tailed Student's t-test, n=3, n.s. : no significant.

532

533 Figure. 4. *Tctex1d2* is important for sperm flagellum formation. (A-D) Periodic acid
534 Schiff hematoxylin (PAS-H) stain of seminiferous tubules of *Tctex1d2* $^{+/+}$ and *Tctex1d2*
535 $^{-/-}$ mice. In stage I-II seminiferous tubules, *Tctex1d2* $^{-/-}$ mice showed layered structures
536 of germ cells (B; yellow box), similar to that in *Tctex1d2* $^{+/+}$ mice (A; yellow box).
537 However, sperm flagella were barely observed in the lumen in *Tctex1d2* $^{-/-}$ mice (B; red
538 box) compared to *Tctex1d2* $^{+/+}$ mice (A; red box arrow). In the lumen of stage VII
539 seminiferous tubules, only a few elongated spermatids were observed in *Tctex1d2* $^{-/-}$
540 mice (D; black box) in contrast to *Tctex1d2* $^{+/+}$ mice (C; black box). Scale bars are
541 50 µm. (E) Hematoxylin and eosin (H&E) stain of the cauda epididymis. Many spermatozoa
542 were observed in *Tctex1d2* $^{+/+}$ mice, whereas only very few spermatozoa were observed
543 in *Tctex1d2* $^{-/-}$ mice. Scale bars are 50 µm. (F) Sperm counts in the cauda epididymis.
544 *Tctex1d2* $^{-/-}$ mice had significantly reduced sperm counts compared to *Tctex1d2* $^{+/+}$ mice.
545 Error bars are means ± S.E. Two-tailed Student's t-test, n=3, $*p < 0.05$. (G) Cauda
546 epididymis sperm observed using phase contrast microscopy. Sperm flagella of *Tctex1d2*
547 $^{-/-}$ mice showed morphological abnormalities. Scale bars are 10 µm. (H) The ratio of
548 sperm with abnormal flagella in the cauda epididymis. Almost all sperm showed abnormal
549 flagella in *Tctex1d2* $^{-/-}$ mice. Error bars are means ± S.E. Two-tailed Student's t-test,
550 n=3, $*p < 0.05$.
551
552 Figure. 5. Abnormal assembly of sperm flagella in *Tctex1d2* $^{-/-}$ mice occurred from step
553 4 round spermatids. (A) Flagella formation in spermiogenesis using ICCs (green:
554 anti-acetylated-α-tubulin, red: PNA lectin, blue: hoechst33342). In *Tctex1d2* $^{+/+}$ mice,
555 flagella elongated as the spermatids differentiated. However, *Tctex1d2* $^{-/-}$ mice showed
556 markedly abnormal flagella after step 4 spermatids. Scale bars are 10 µm. (B)
557 Observation of the internal structure of the flagella of spermatids using transmission
558 electron microscopy. In *Tctex1d2* $^{+/+}$ mice, microtubule 9+2 structures and other
559 structures were neatly aligned in the axonemes. In contrast, in *Tctex1d2* $^{-/-}$ mice, the
560 internal structure of the axonemes were disorganized. The 9+2 structures, inner dynein
561 arm (IDA), outer dynein arm (ODA), outer dense fiber (ODF), and fibrous sheath (FS)
562 were not aligned properly. Scale bars are 250 nm. MS, mitochondrial sheath; DMTs,
563 doublet microtubules; ODF, outer dense fibers; FS, fibrous sheath; ODA, outer dynein
564 arm; IDA, inner dynein arm; MTs, microtubule (not doublet).
565
566 Figure. 6. TCTEX1D2 played a role in the assembly of cytoplasmic dynein 2 subunits.
567 (A) Expression analysis of WDR60 in *Tctex1d2* $^{-/-}$ mice using ICC (green: WDR60, red:
568 acetylated-α-tubulin, blue: hoechst33342). There was no expression of WDR60 in

569 flagella of round spermatids in *Tctex1d2* $^{+/+}$ mice. In elongated spermatids, abnormal
570 expression was observed in *Tctex1d2* $^{-/-}$ mice (top: loss of signal, bottom: ectopic
571 expression). (B) Expression analysis of WDR34 in *Tctex1d2* $^{-/-}$ mice using ICC (green:
572 WDR34, red: acetylated-α-tubulin, blue: hoechst33342). There was no expression of
573 WDR34 was in flagella of round spermatids, as seen with WDR60. In elongated spermatids,
574 abnormal expression was observed in *Tctex1d2* $^{-/-}$ mice (top: loss of signal, bottom:
575 ectopic expression). (C) Expression analysis of DYNLT1 in *Tctex1d2* $^{-/-}$ mice using ICC
576 (green: DYNLT1, red: acetylated-α-tubulin, blue: hoechst33342). The signal was
577 decreased in round spermatids and absent in elongated spermatids in *Tctex1d2* $^{-/-}$ mice.
578 RST, round spermatid; EST, elongated spermatid. (D) Schematic diagram of the defect
579 of cytoplasmic dynein 2 subunits in *Tctex1d2* $^{-/-}$ mice. In*Tctex1d2* $^{-/-}$ mice elongated
580 spermatids, DYNC2LI1, WDR60, WDR34 and DYNLT1 showed abnormal localization and were
581 not assembled in the cytoplasmic dynein 2 complex.
582
583
584 Supplementary Material
585 Supplement figure. 1. Generation of *Tctex1d2* - 3×FLAG mice. (A) Schematic
586 representation of *Tctex1d2* - 3×FLAG mice and the results of Sanger sequencing.
587 3×FLAG was knocked immediately after the start codon. Sanger sequencing indicated
588 that the 3 × FLAG nucleotide sequence was knocked-in within the target region. (B)
589 PAS-H staining of seminiferous tubules of WT and *Tctex1d2* - 3×FLAG mice. Scale bars
590 are 50 μm. (C) Phase contrast microscopy of cauda epididymis sperm. There were no
591 differences of sperm morphology between WT and *Tctex1d2* - 3×FLAG mice. Scale bars
592 are 10 μm.
593
594 Supplement figure. 2. TCTEX1D2 was also localized to motile cilia. IHC of WT and
595 *Tctex1d2* - 3×FLAG in tissues with motile cilia to analyze the expression of TCTEX1D2
596 (green: anti-FLAG, red: anti-acetylated-α-tubulin, blue: hoechst33342). (A)
597 ventricle, (B) trachea, and (C) oviduct. TCTEX1D2 is expressed in the cilia of the
598 ventricle, trachea, and oviduct. (*); The signals found in the epithelial cells of
599 each tissue are non-specific. Scale bars are 10 μm.
600
601 Supplement figure. 3. Motile cilia in *Tctex1d2* $^{-/-}$ mice were normal. H&E stain of tissues
602 with motile cilia. (A) ventricle, (B) trachea, and (C) oviduct. In motile cilia, there
603 were no differences in morphology between *Tctex1d2* $^{+/+}$ and *Tctex1d2* $^{-/-}$ mice. Scale bars
604 are 20 μm.

605

606 Supplement figure. 4. *Tctex1d2* $^{-/-}$ mice exhibited abnormal protein localization in the
607 IFT system. Expression analysis of cytoplasmic dynein 2 (DYNC2H1 and DYNC2LI1),
608 kinesin 2 (KIF3A), and IFT proteins (IFT88, 140) in elongated spermatids of *Tctex1d2*
609 $^{-/-}$ mice using ICC (red: anti-acetylated-α-tubulin, Blue: hoechst33342). (A) IFT88,
610 (B) DYNC2LI1, (C) IFT140, (D) DYNC2H1, and (E) KIF3A. IFT88 and DYNC2LI1 showed a
611 reduced signal and were ectopically expressed in the flagella of *Tctex1d2* $^{-/-}$ mice,
612 whereas IFT140, DYNC2H1, and KIF3A were expressed normally in *Tctex1d2* $^{-/-}$ mice. Scale
613 bars are 10 μm.

614

615 Supplement figure. 5. The IFT system was normal in the cilia of the ventricles.
616 Expression analysis of cytoplasmic dynein 2 (DYNLT1) and IFT protein (IFT88) in the
617 ventricle of *Tctex1d2* $^{-/-}$ mice using IHC (red: anti-acetylated-α-tubulin, blue:
618 hoechst33342). In *Tctex1d2* $^{-/-}$ mice, the two proteins showed abnormal expression in
619 the flagella of elongated spermatids, but not in the ventricle. Scale bars are 10
620 μm.

621

Funding

This work was supported by the JSPS KAKENHI (19H01142 to K.T., 23K21259 to K.H.) and JST FOREST Program (JPMJFR2018 to K.H.) and JST SPRING (JPMJSP2114 to R.H.).

Author contributions

Ryua Harima, Conceptualization, Methodology, Validation, Formal analysis, Investigation, Resources, Data curation, Writing - original draft preparation, Writing - review & editing, Visualization, Project administration, Funding acquisition; Kenshiro Hara, Resources, Writing - original draft preparation, Writing - review & editing, Funding acquisition; Kentaro Tanemura; Resources, Supervision, Writing - original draft preparation, Writing - review & editing, Funding acquisition.

Acknowledgments

We would like to thank Editage (www.editage.com) for English language editing.

637 Reference

638 1. Gibbons, I.R. (1981). Cilia and flagella of eukaryotes. J Cell Biol *91*, 107s-124s.
639 10.1083/jcb.91.3.107s.
640 2. Carvalho-Santos, Z., Azimzadeh, J., Pereira-Leal, J.B., and Bettencourt-Dias, M.
641 (2011). Evolution: Tracing the origins of centrioles, cilia, and flagella. J Cell
642 Biol *194*, 165-175. 10.1083/jcb.201011152.
643 3. Lindemann, C.B., and Lesich, K.A. (2016). Functional anatomy of the mammalian sperm
644 flagellum. Cytoskeleton (Hoboken) *73*, 652-669. 10.1002/cm.21338.
645 4. Satir, P., and Christensen, S.T. (2007). Overview of structure and function of
646 mammalian cilia. Annu Rev Physiol *69*, 377-400.
647 10.1146/annurev.physiol.69.040705.141236.
648 5. Allen, R.D. (1968). A reinvestigation of cross-sections of cilia. J Cell Biol *37*,
649 825-831. 10.1083/jcb.37.3.825.
650 6. Luck, D.J. (1984). Genetic and biochemical dissection of the eucaryotic flagellum.
651 J Cell Biol *98*, 789-794. 10.1083/jcb.98.3.789.
652 7. Porter, M.E., and Sale, W.S. (2000). The 9 + 2 axoneme anchors multiple inner arm
653 dyneins and a network of kinases and phosphatases that control motility. J Cell
654 Biol *151*, F37-42. 10.1083/jcb.151.5.f37.
655 8. Pazour, G.J., Wilkerson, C.G., and Witman, G.B. (1998). A dynein light chain is
656 essential for the retrograde particle movement of intraflagellar transport (IFT).
657 J Cell Biol *141*, 979-992. 10.1083/jcb.141.4.979.
658 9. Rosenbaum, J.L., and Witman, G.B. (2002). Intraflagellar transport. Nat Rev Mol
659 Cell Biol *3*, 813-825. 10.1038/nrm952.
660 10. Mohri, H., Inaba, K., Ishijima, S., and Baba, S.A. (2012). Tubulin-dynein system
661 in flagellar and ciliary movement. Proc Jpn Acad Ser B Phys Biol Sci *88*, 397-415.
662 10.2183/pjab.88.397.
663 11. Asante, D., Stevenson, N.L., and Stephens, D.J. (2014). Subunit composition of
664 the human cytoplasmic dynein-2 complex. J Cell Sci *127*, 4774-4787.
665 10.1242/jcs.159038.
666 12. Pfister, K.K., Shah, P.R., Hummerich, H., Russ, A., Cotton, J., Annuar, A.A., King,
667 S.M., and Fisher, E.M. (2006). Genetic analysis of the cytoplasmic dynein subunit
668 families. PLoS Genet *2*, e1. 10.1371/journal.pgen.0020001.
669 13. Roberts, A.J., Kon, T., Knight, P.J., Sutoh, K., and Burgess, S.A. (2013).
670 Functions and mechanics of dynein motor proteins. Nat Rev Mol Cell Biol *14*, 713-726.
671 10.1038/nrm3667.
672 14. Pazour, G.J., Dickert, B.L., and Witman, G.B. (1999). The DHC1b (DHC2) isoform

673 of cytoplasmic dynein is required for flagellar assembly. J Cell Biol *144*, 473-481.
674 10.1083/jcb.144.3.473.
675 15. Summers, K.E., and Gibbons, I.R. (1971). Adenosine triphosphate-induced sliding
676 of tubules in trypsin-treated flagella of sea-urchin sperm. Proc Natl Acad Sci
677 U S A *68*, 3092-3096. 10.1073/pnas.68.12.3092.
678 16. Inaba, K., and Mizuno, K. (2016). Sperm dysfunction and ciliopathy. Reprod Med
679 Biol *15*, 77-94. 10.1007/s12522-015-0225-5.
680 17. Mikami, A., Tynan, S.H., Hama, T., Luby-Phelps, K., Saito, T., Crandall, J.E.,
681 Besharse, J.C., and Vallee, R.B. (2002). Molecular structure of cytoplasmic dynein
682 2 and its distribution in neuronal and ciliated cells. J Cell Sci *115*, 4801-4808.
683 10.1242/jcs.00168.
684 18. Vuolo, L., Stevenson, N.L., Mukhopadhyay, A.G., Roberts, A.J., and Stephens, D.J.
685 (2020). Cytoplasmic dynein-2 at a glance. J Cell Sci *133*. 10.1242/jcs.240614.
686 19. Cole, D.G. (2003). The intraflagellar transport machinery of Chlamydomonas
687 reinhardtii. Traffic *4*, 435-442. 10.1034/j.1600-0854.2003.t01-1-00103.x.
688 20. Signor, D., Wedaman, K.P., Orozco, J.T., Dwyer, N.D., Bargmann, C.I., Rose, L.S.,
689 and Scholey, J.M. (1999). Role of a class DHC1b dynein in retrograde transport
690 of IFT motors and IFT raft particles along cilia, but not dendrites, in chemosensory
691 neurons of living Caenorhabditis elegans. J Cell Biol *147*, 519-530.
692 10.1083/jcb.147.3.519.
693 21. Toropova, K., Zalyte, R., Mukhopadhyay, A.G., Mladenov, M., Carter, A.P., and
694 Roberts, A.J. (2019). Structure of the dynein-2 complex and its assembly with
695 intraflagellar transport trains. Nat Struct Mol Biol *26*, 823-829.
696 10.1038/s41594-019-0286-y.
697 22. Reck-Peterson, S.L., Redwine, W.B., Vale, R.D., and Carter, A.P. (2018). The
698 cytoplasmic dynein transport machinery and its many cargoes. Nat Rev Mol Cell Biol
699 *19*, 382-398. 10.1038/s41580-018-0004-3.
700 23. Braschi, B., Omran, H., Witman, G.B., Pazour, G.J., Pfister, K.K., Bruford, E.A.,
701 and King, S.M. (2022). Consensus nomenclature for dyneins and associated assembly
702 factors. J Cell Biol *221*. 10.1083/jcb.202109014.
703 24. Viswanadha, R., Sale, W.S., and Porter, M.E. (2017). Ciliary Motility: Regulation
704 of Axonemal Dynein Motors. Cold Spring Harb Perspect Biol *9*.
705 10.1101/cshperspect.a018325.
706 25. Konno, A., Shiba, K., Cai, C., and Inaba, K. (2015). Branchial cilia and sperm
707 flagella recruit distinct axonemal components. PLoS One *10*, e0126005.
708 10.1371/journal.pone.0126005.

709 26. Sarpal, R., Todi, S.V., Sivan-Loukianova, E., Shirolikar, S., Subramanian, N.,
710 Raff, E.C., Erickson, J.W., Ray, K., and Eberl, D.F. (2003). Drosophila KAP
711 interacts with the kinesin II motor subunit KLP64D to assemble chordotonal sensory
712 cilia, but not sperm tails. Curr Biol *13*, 1687-1696. 10.1016/j.cub.2003.09.025.
713 27. Han, Y.G., Kwok, B.H., and Kernan, M.J. (2003). Intraflagellar transport is
714 required in Drosophila to differentiate sensory cilia but not sperm. Curr Biol
715 *13*, 1679-1686. 10.1016/j.cub.2003.08.034.
716 28. Gholkar, A.A., Senese, S., Lo, Y.C., Capri, J., Deardorff, W.J., Dharmarajan, H.,
717 Contreras, E., Hodara, E., Whitelegge, J.P., Jackson, P.K., and Torres, J.Z. (2015).
718 Tctex1d2 associates with short-rib polydactyly syndrome proteins and is required
719 for ciliogenesis. Cell Cycle *14*, 1116-1125. 10.4161/15384101.2014.985066.
720 29. Schmidts, M., Hou, Y., Cortés, C.R., Mans, D.A., Huber, C., Boldt, K., Patel, M.,
721 van Reeuwijk, J., Plaza, J.M., van Beersum, S.E., et al. (2015). TCTEX1D2 mutations
722 underlie Jeune asphyxiating thoracic dystrophy with impaired retrograde
723 intraflagellar transport. Nat Commun *6*, 7074. 10.1038/ncomms8074.
724 30. Hamada, Y., Tsurumi, Y., Nozaki, S., Katoh, Y., and Nakayama, K. (2018).
725 Interaction of WDR60 intermediate chain with TCTEX1D2 light chain of the dynein-2
726 complex is crucial for ciliary protein trafficking. Mol Biol Cell *29*, 1628-1639.
727 10.1091/mbc.E18-03-0173.
728 31. Green, C.D., Ma, Q., Manske, G.L., Shami, A.N., Zheng, X., Marini, S., Moritz,
729 L., Sultan, C., Gurczynski, S.J., Moore, B.B., et al. (2018). A Comprehensive
730 Roadmap of Murine Spermatogenesis Defined by Single-Cell RNA-Seq. Dev Cell *46*,
731 651-667.e610. 10.1016/j.devcel.2018.07.025.
732 32. DiBella, L.M., Smith, E.F., Patel-King, R.S., Wakabayashi, K., and King, S.M.
733 (2004). A novel Tctex2-related light chain is required for stability of inner
734 dynein arm I1 and motor function in the Chlamydomonas flagellum. J Biol Chem *279*,
735 21666-21676. 10.1074/jbc.M313540200.
736 33. Brokaw, C.J., and Kamiya, R. (1987). Bending patterns of Chlamydomonas flagella:
737 IV. Mutants with defects in inner and outer dynein arms indicate differences in
738 dynein arm function. Cell Motil Cytoskeleton *8*, 68-75. 10.1002/cm.970080110.
739 34. Huang, B., Piperno, G., and Luck, D.J. (1979). Paralyzed flagella mutants of
740 Chlamydomonas reinhardtii. Defective for axonemal doublet microtubule arms. J Biol
741 Chem *254*, 3091-3099.
742 35. Yamamoto, R., Obbineni, J.M., Alford, L.M., Ide, T., Owa, M., Hwang, J., Kon, T.,
743 Inaba, K., James, N., King, S.M., et al. (2017). Chlamydomonas DYX1C1/PF23 is
744 essential for axonemal assembly and proper morphology of inner dynein arms. PLoS

745 Genet *13*, e1006996. 10.1371/journal.pgen.1006996.
746 36. Yamamoto, R., Yanagi, S., Nagao, M., Yamasaki, Y., Tanaka, Y., Sale, W.S., Yagi,
747 T., and Kon, T. (2020). Mutations in PIH proteins MOT48, TWI1 and PF13 define common
748 and unique steps for preassembly of each, different ciliary dynein. PLoS Genet
749 *16*, e1009126. 10.1371/journal.pgen.1009126.
750 37. Cole, D.G., Diener, D.R., Himelblau, A.L., Beech, P.L., Fuster, J.C., and Rosenbaum,
751 J.L. (1998). Chlamydomonas kinesin-II-dependent intraflagellar transport (IFT):
752 IFT particles contain proteins required for ciliary assembly in Caenorhabditis
753 elegans sensory neurons. J Cell Biol *141*, 993-1008. 10.1083/jcb.141.4.993.
754 38. Stepanek, L., and Pigino, G. (2016). Microtubule doublets are double-track
755 railways for intraflagellar transport trains. Science *352*, 721-724.
756 10.1126/science.aaf4594.
757 39. Nachury, M.V., Loktev, A.V., Zhang, Q., Westlake, C.J., Peränen, J., Merdes, A.,
758 Slusarski, D.C., Scheller, R.H., Bazan, J.F., Sheffield, V.C., and Jackson, P.K.
759 (2007). A core complex of BBS proteins cooperates with the GTPase Rab8 to promote
760 ciliary membrane biogenesis. Cell *129*, 1201-1213. 10.1016/j.cell.2007.03.053.
761 40. Wu, C., Li, J., Peterson, A., Tao, K., and Wang, B. (2017). Loss of dynein-2
762 intermediate chain Wdr34 results in defects in retrograde ciliary protein
763 trafficking and Hedgehog signaling in the mouse. Hum Mol Genet *26*, 2386-2397.
764 10.1093/hmg/ddx127.
765 41. Vuolo, L., Stevenson, N.L., Heesom, K.J., and Stephens, D.J. (2018). Dynein-2
766 intermediate chains play crucial but distinct roles in primary cilia formation
767 and function. Elife *7*. 10.7554/eLife.39655.
768 42. Nakayama, K., and Katoh, Y. (2018). Ciliary protein trafficking mediated by IFT
769 and BBSome complexes with the aid of kinesin-2 and dynein-2 motors. J Biochem *163*,
770 155-164. 10.1093/jb/mvx087.
771 43. Kessler, K., Wunderlich, I., Uebe, S., Falk, N.S., Gießl, A., Brandstätter, J.H.,
772 Popp, B., Klinger, P., Ekici, A.B., Sticht, H., et al. (2015). DYNC2LI1 mutations
773 broaden the clinical spectrum of dynein-2 defects. Sci Rep *5*, 11649.
774 10.1038/srep11649.
775 44. Fu, G., Scarbrough, C., Song, K., Phan, N., Wirschell, M., and Nicastro, D. (2021).
776 Structural organization of the intermediate and light chain complex of
777 Chlamydomonas ciliary I1 dynein. Faseb j *35*, e21646. 10.1096/fj.202001857R.
778 45. Lu, S., Gu, Y., Wu, Y., Yang, S., Li, C., Meng, L., Yuan, W., Jiang, T., Zhang,
779 X., Li, Y., et al. (2021). Bi-allelic variants in human WDR63 cause male infertility
780 via abnormal inner dynein arms assembly. Cell Discov *7*, 110.

781 10.1038/s41421-021-00327-5.
782 46. Urbanska, P., Song, K., Joachimiak, E., Krzemien-Ojak, L., Koprowski, P.,
783 Hennessey, T., Jerka-Dziadosz, M., Fabczak, H., Gaertig, J., Nicastro, D., and
784 Wloga, D. (2015). The CSC proteins FAP61 and FAP251 build the basal substructures
785 of radial spoke 3 in cilia. Mol Biol Cell *26*, 1463-1475. 10.1091/mbc.E14-11-1545.
786 47. Liu, S., Zhang, J., Kherraf, Z.E., Sun, S., Zhang, X., Cazin, C., Coutton, C.,
787 Zouari, R., Zhao, S., Hu, F., et al. (2021). CFAP61 is required for sperm flagellum
788 formation and male fertility in human and mouse. Development *148*.
789 10.1242/dev.199805.
790 48. Coutton, C., Escoffier, J., Martinez, G., Arnoult, C., and Ray, P.F. (2015).
791 Teratozoospermia: spotlight on the main genetic actors in the human. Hum Reprod
792 Update *21*, 455-485. 10.1093/humupd/dmv020.
793 49. Ben Khelifa, M., Coutton, C., Zouari, R., Karaouzène, T., Rendu, J., Bidart, M.,
794 Yassine, S., Pierre, V., Delaroche, J., Hennebicq, S., et al. (2014). Mutations
795 in DNAH1, which encodes an inner arm heavy chain dynein, lead to male infertility
796 from multiple morphological abnormalities of the sperm flagella. Am J Hum Genet
797 *94*, 95-104. 10.1016/j.ajhg.2013.11.017.
798 50. Touré, A., Martinez, G., Kherraf, Z.E., Cazin, C., Beurois, J., Arnoult, C., Ray,
799 P.F., and Coutton, C. (2021). The genetic architecture of morphological
800 abnormalities of the sperm tail. Hum Genet *140*, 21-42. 10.1007/s00439-020-02113-x.
801 51. Liu, C., He, X., Liu, W., Yang, S., Wang, L., Li, W., Wu, H., Tang, S., Ni, X.,
802 Wang, J., et al. (2019). Bi-allelic Mutations in TTC29 Cause Male Subfertility
803 with Asthenoteratospermia in Humans and Mice. Am J Hum Genet *105*, 1168-1181.
804 10.1016/j.ajhg.2019.10.010.
805 52. Lorès, P., Dacheux, D., Kherraf, Z.E., Nsota Mbango, J.F., Coutton, C., Stouvenel,
806 L., Ialy-Radio, C., Amiri-Yekta, A., Whitfield, M., Schmitt, A., et al. (2019).
807 Mutations in TTC29, Encoding an Evolutionarily Conserved Axonemal Protein, Result
808 in Asthenozoospermia and Male Infertility. Am J Hum Genet *105*, 1148-1167.
809 10.1016/j.ajhg.2019.10.007.
810 53. Gurumurthy, C.B., Sato, M., Nakamura, A., Inui, M., Kawano, N., Islam, M.A.,
811 Ogiwara, S., Takabayashi, S., Matsuyama, M., Nakagawa, S., et al. (2019). Creation
812 of CRISPR-based germline-genome-engineered mice without ex vivo handling of
813 zygotes by i-GONAD. Nat Protoc *14*, 2452-2482. 10.1038/s41596-019-0187-x.
814 54. Hiradate, Y., Harima, R., Yanai, R., Hara, K., Nagasawa, K., Osada, M., Kobayashi,
815 T., Matsuyama, M., Kanno, S.I., Yasui, A., and Tanemura, K. (2022). Loss of Axdnd1
816 causes sterility due to impaired spermatid differentiation in mice. Reprod Med

Biol *21*, e12452. 10.1002/rmb2.12452.

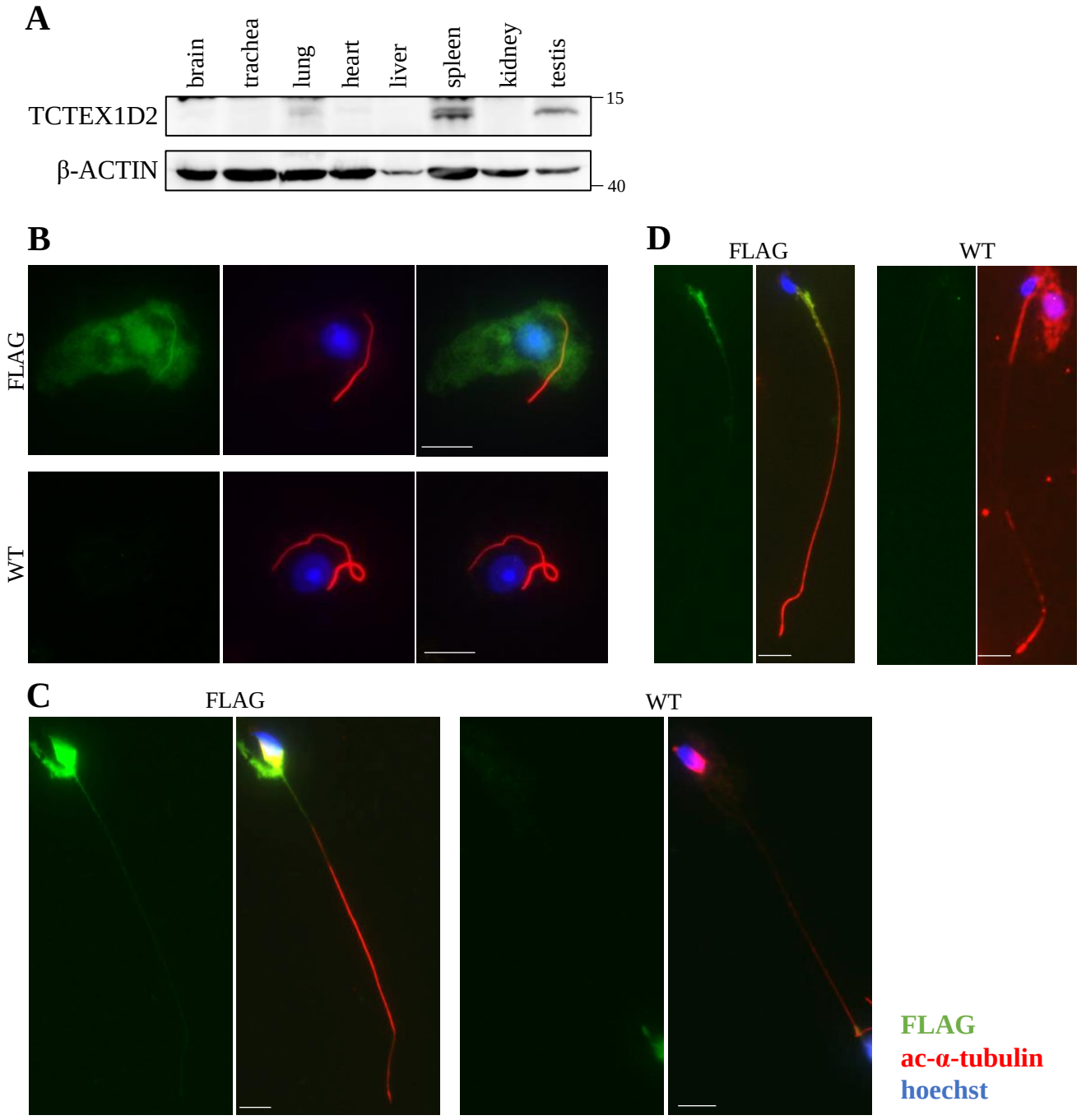
A
brain
trachea
lung
heart
liver
spleen
kidney
testis
TCTEX1D2
15
β-ACTIN
40
B
FLAG
WT
D
FLAG
WT
C
FLAG
WT
FLAG
ac-α-tubulin
hoechst

figure. 1

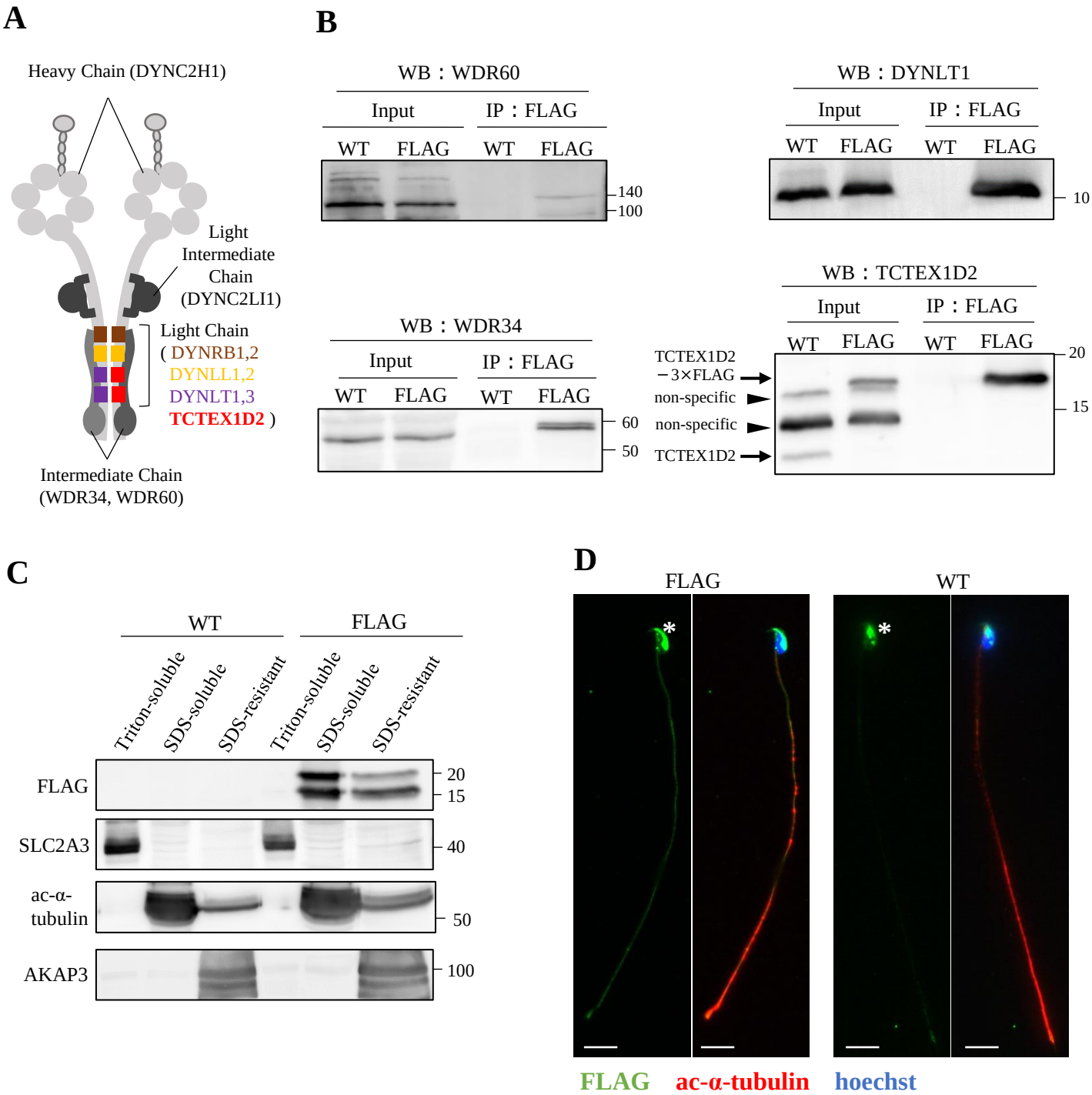
A
Heavy Chain (DYNC2H1)
Light Intermediate Chain (DYNC2LI1)
Light Chain
(DYNRB1,2
DYNLL1,2
DYNLT1,3
TCTEX1D2)
Intermediate Chain (WDR34, WDR60)
B
WB : WDR60
Input
IP : FLAG
WT
FLAG
WT
FLAG
140
100
WB : DYNLT1
10
WB : WDR34
60
50
WB : TCTEX1D2
TCTEX1D2 −3×FLAG
non-specific
non-specific
TCTEX1D2
20
15
C
WT
FLAG
Triton-soluble
SDS-soluble
SDS-resistant
FLAG
SLC2A3
ac-α-tubulin
AKAP3
20
15
40
50
100
D
FLAG
WT
FLAG
ac-α-tubulin
hoechst
E
WB : WDR78
WB : WDR63
100

figure. 2

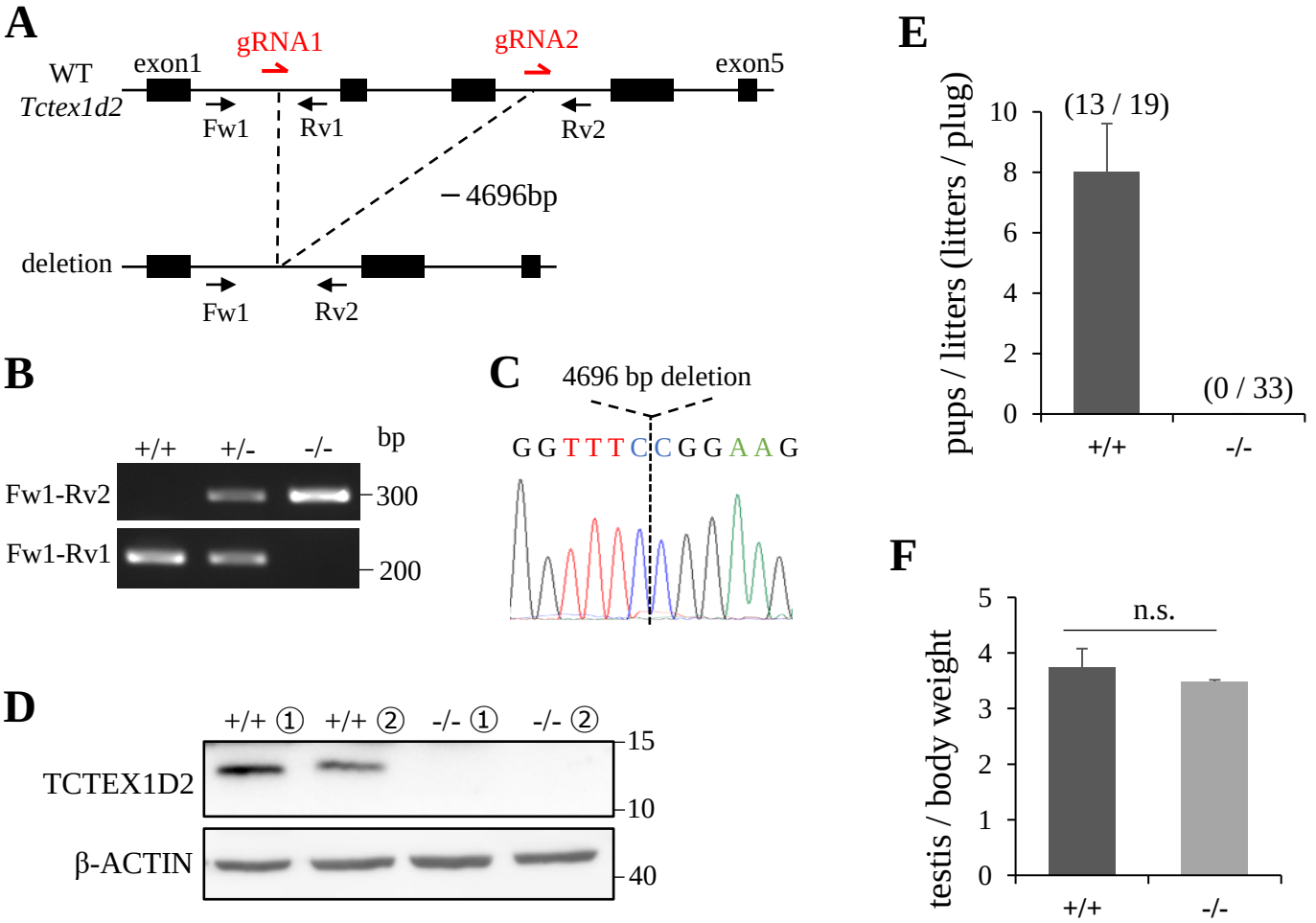
A
WT
Tctex1d2
exon1
gRNA1
gRNA2
exon5
Fw1
Rv1
Rv2
−4696bp
deletion
Fw1
Rv2
B
+/+
+/-
-/-
bp
Fw1-Rv2
Fw1-Rv1
300
200
C
4696 bp deletion
G G T T T C C G G A A G
D
+/+ ①
+/+ ②
-/- ①
-/- ②
TCTEX1D2
β-ACTIN
15
10
40
E
pups / litters (litters / plug)
10
8
6
4
2
0
(13 / 19)
(0 / 33)
+/+
-/-
F
testis / body weight
5
4
3
2
1
0
n.s.
+/+
-/-

figure. 3

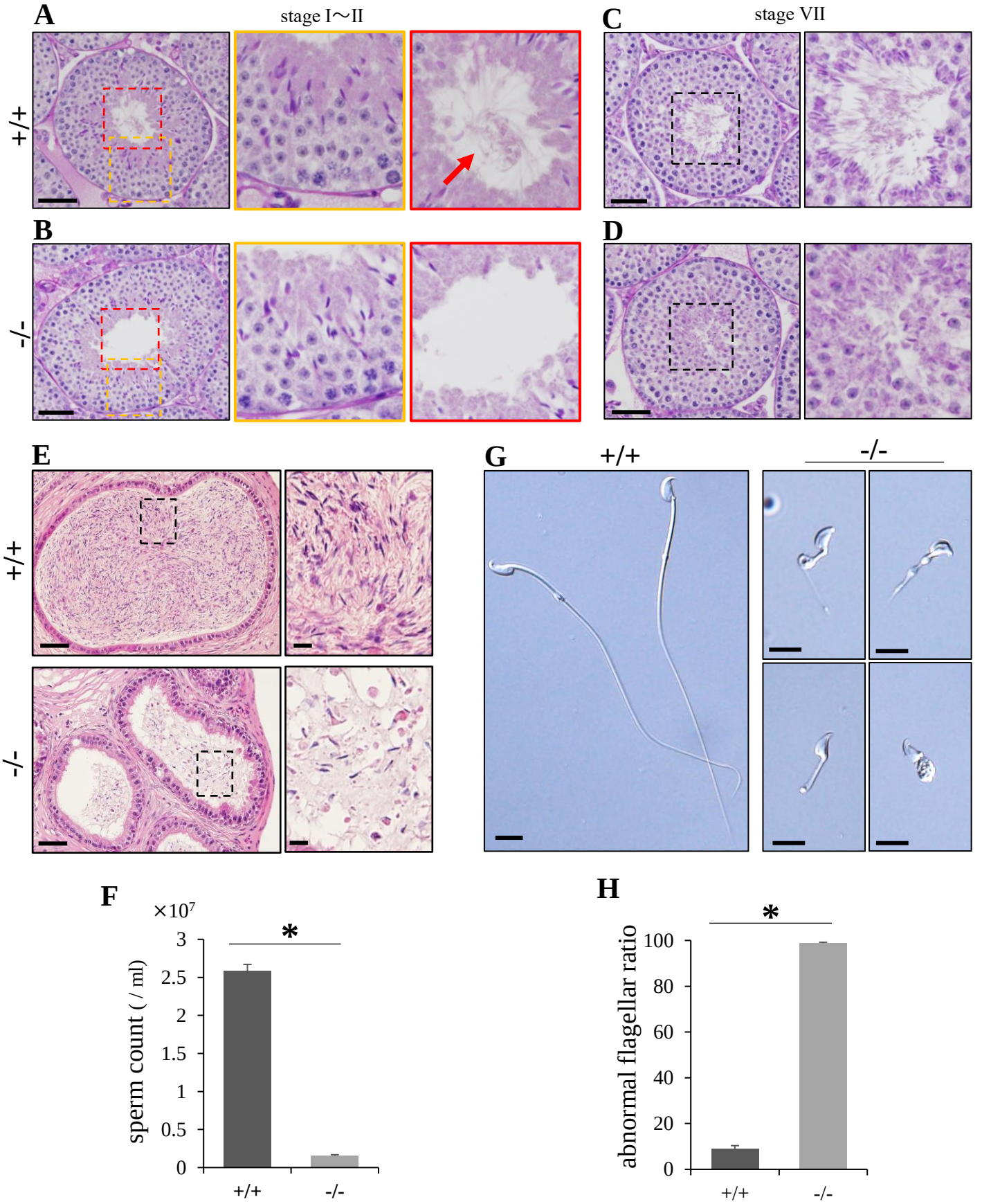
A
stage I～II
C
stage VII
+/+
B
D
-/-
E
+/+
-/-
G
+/+
-/-
F
×10^7
sperm count (/ ml)
3
2.5
2
1.5
1
0.5
0
*
+/+
-/-
H
abnormal flagellar ratio
100
80
60
40
20
0
*
+/+
-/-

figure. 4

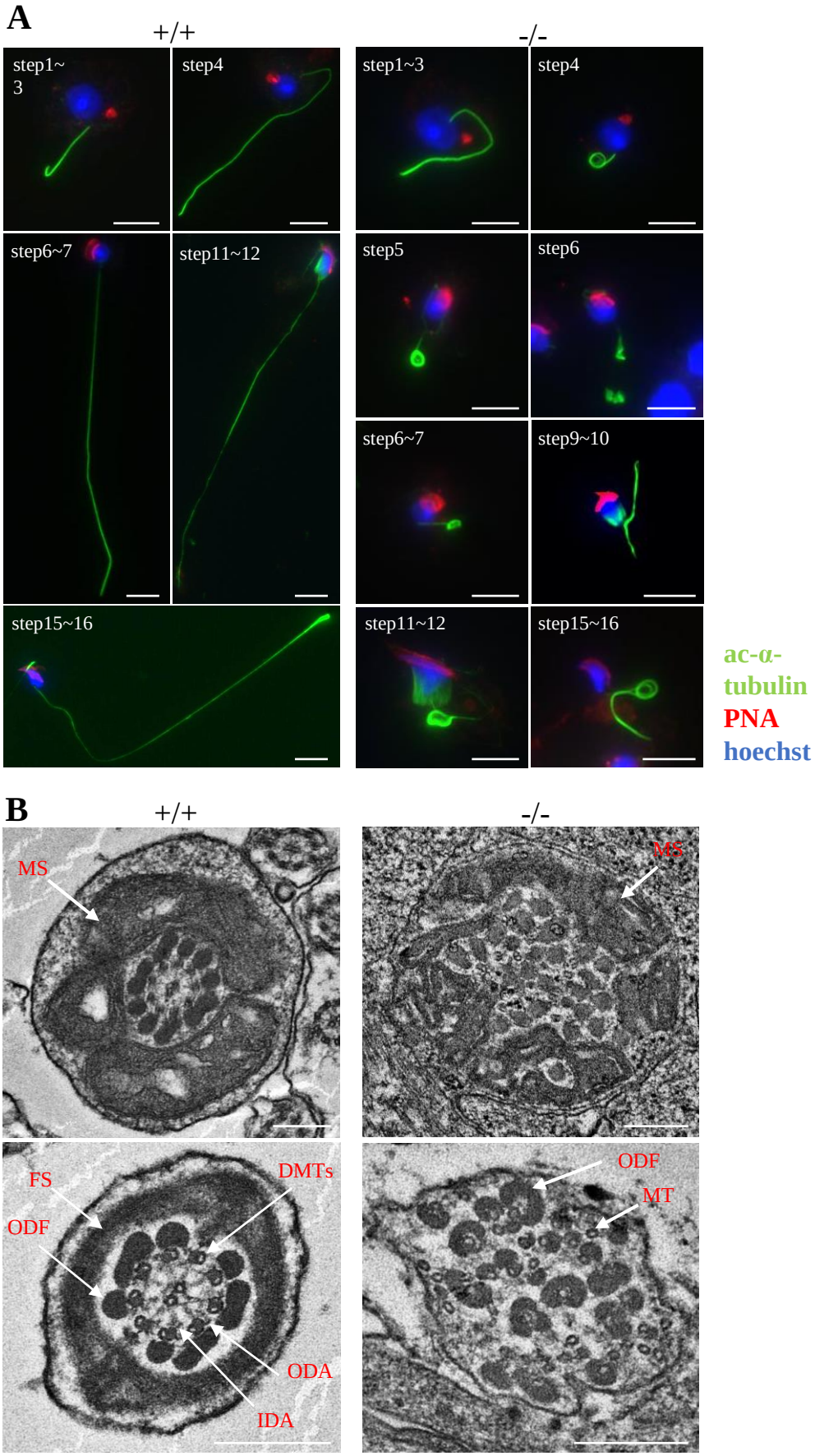
A
+/+
-/-
step1~3
step4
step6~7
step11~12
step15~16
step1~3
step4
step5
step6
step6~7
step9~10
step11~12
step15~16
ac-α-tubulin
PNA
hoechst
B
+/+
-/-
MS
MS
FS
DMTs
ODF
ODA
IDA
ODF
MT

figure. 5

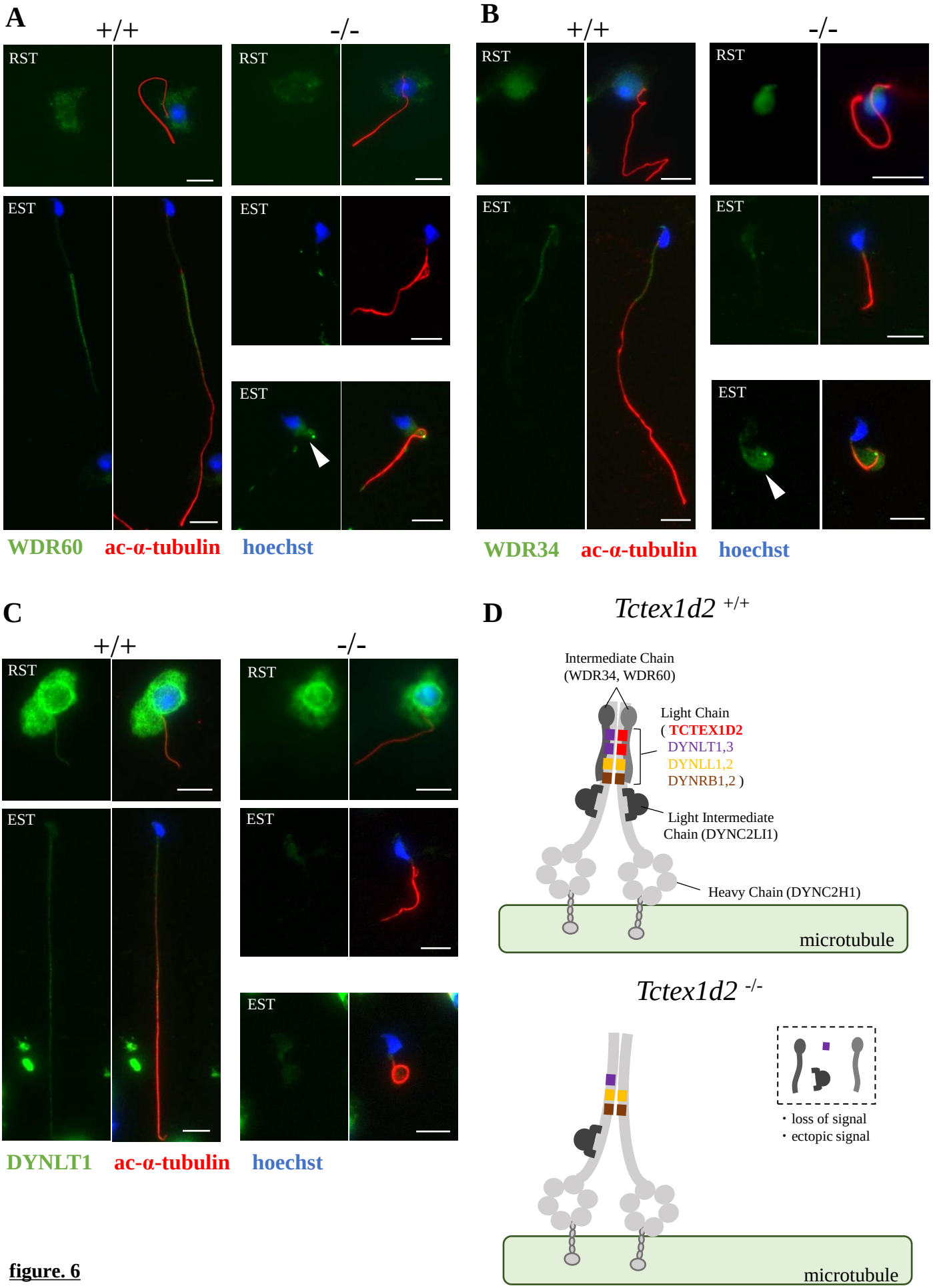
A
+/+
-/-
RST
EST
WDR60
ac-α-tubulin
hoechst
B
WDR34
C
DYNLT1
D
Tctex1d2 +/+
Intermediate Chain
(WDR34, WDR60)
Light Chain
(TCTEX1D2
DYNLT1,3
DYNLL1,2
DYNRB1,2)
Light Intermediate
Chain (DYNC2LI1)
Heavy Chain (DYNC2H1)
microtubule
Tctex1d2 -/-
・loss of signal
・ectopic signal

figure. 6

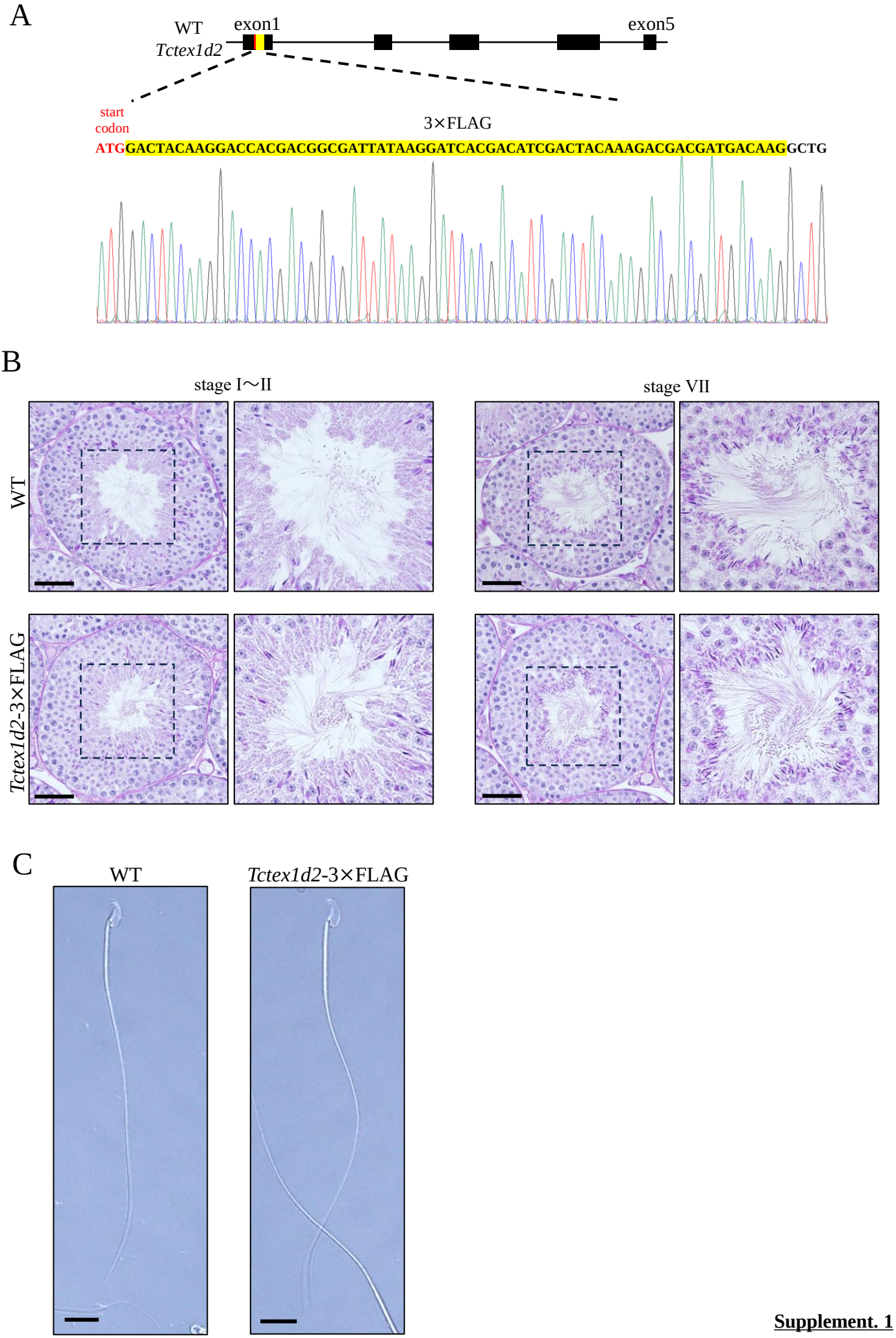

Supplement. 1

A

ventricle

FLAG WT

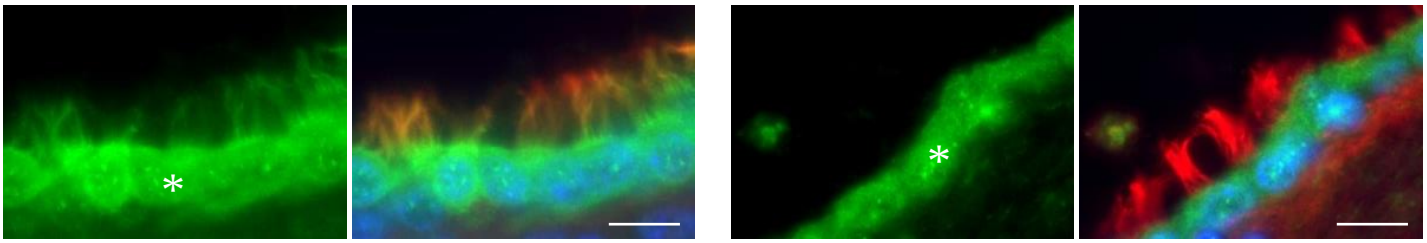

B

trachea

FLAG WT

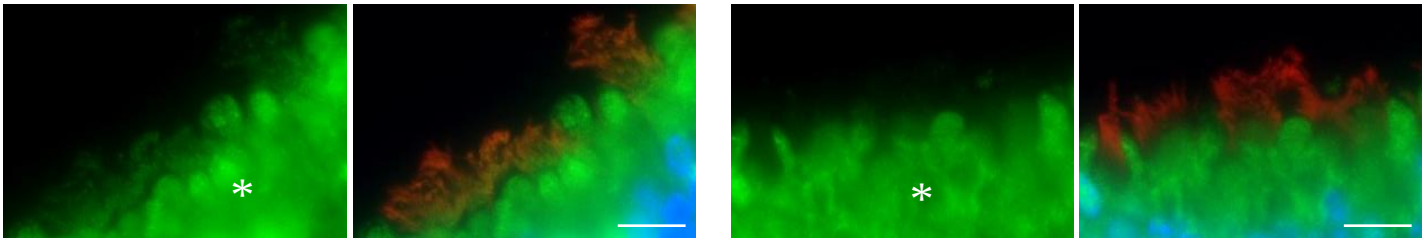

C

oviduct

FLAG WT

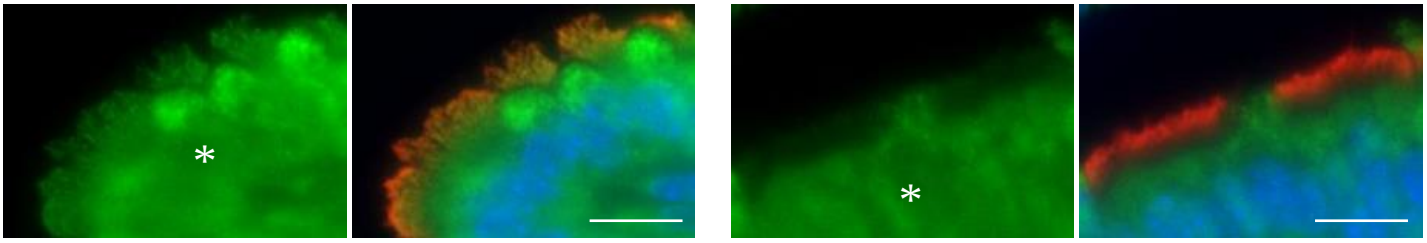

FLAG **ac-α-tubulin** **hoechst**

Supplement. 2

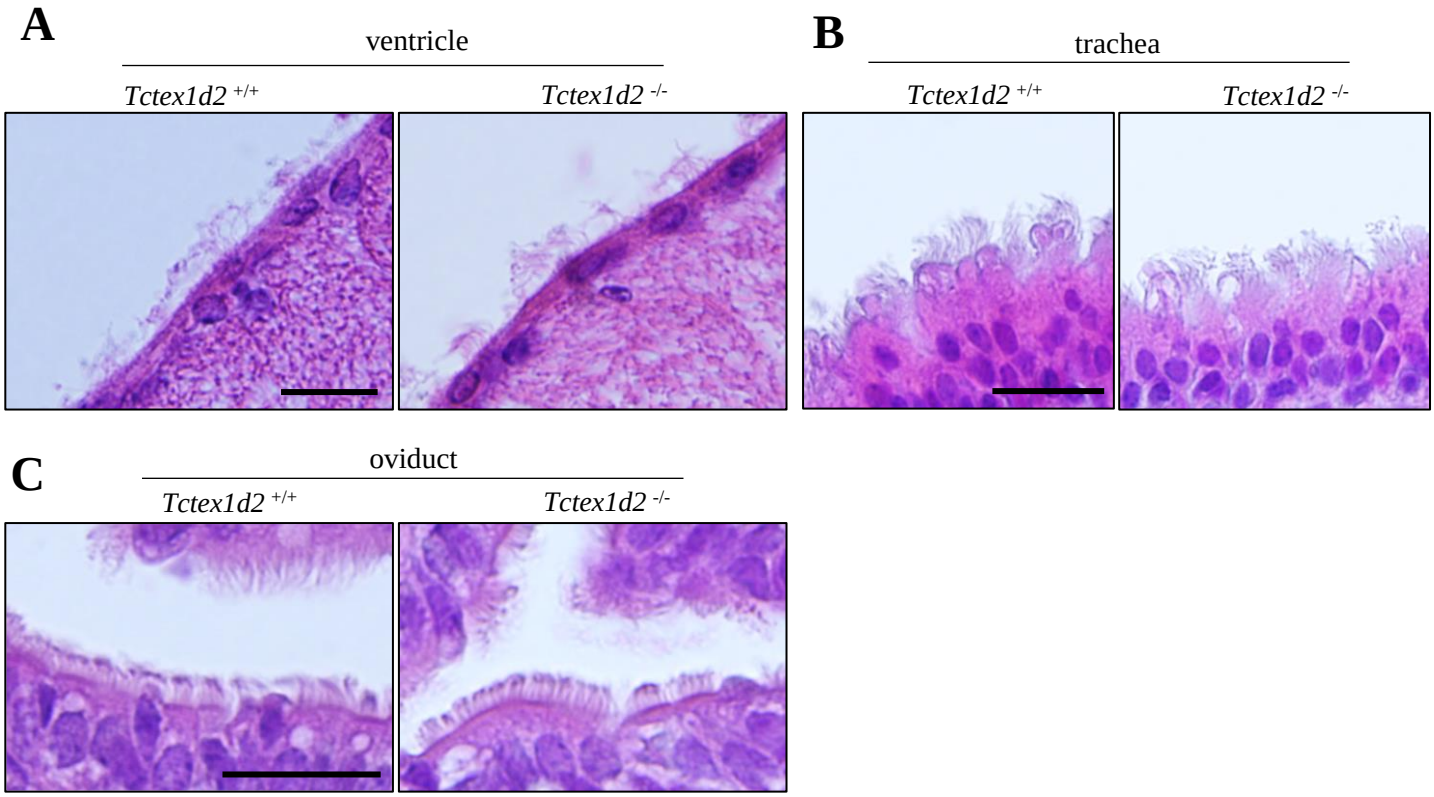

Supplement. 3

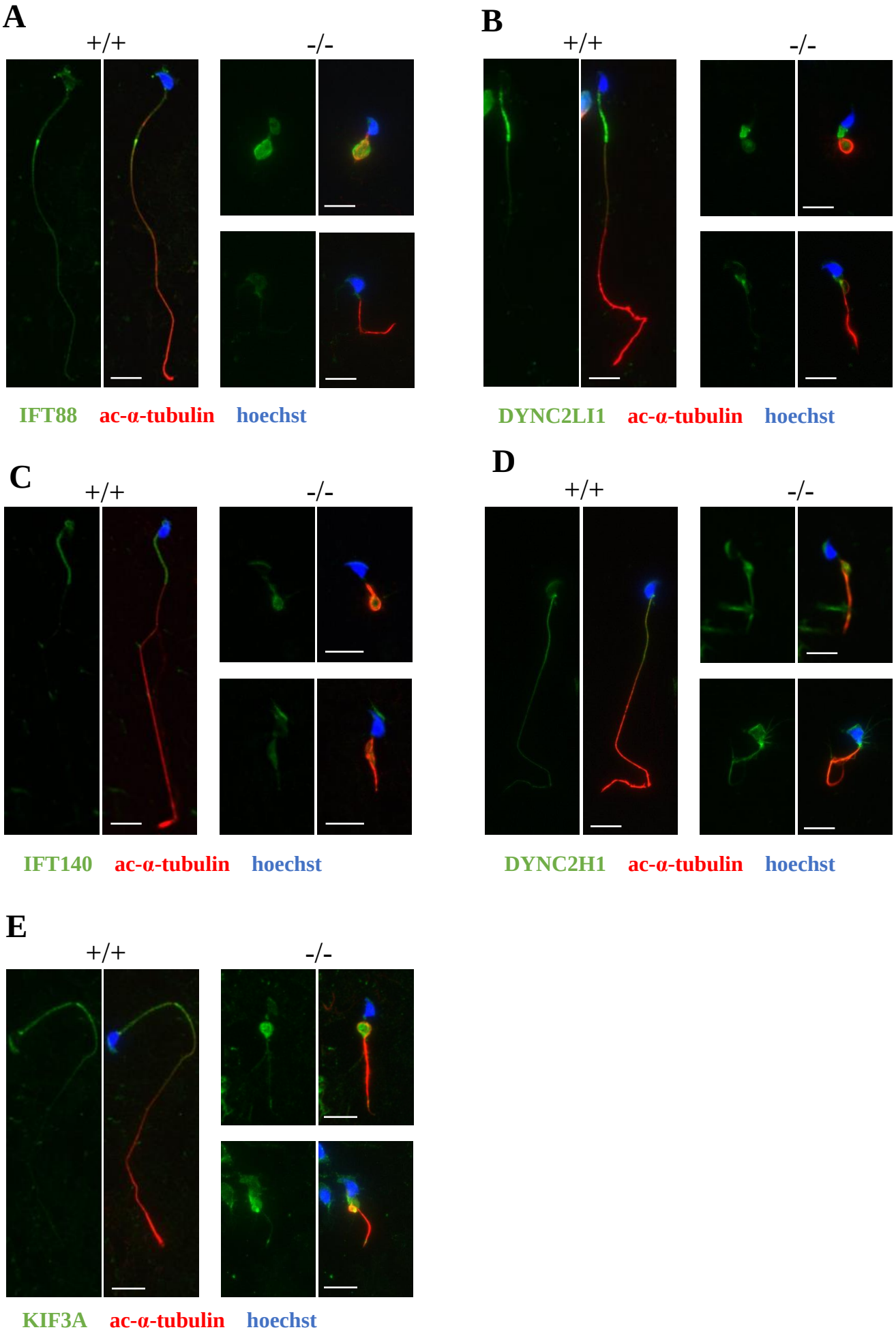

Supplement. 4

A

DYNLT1

+/+ -/-

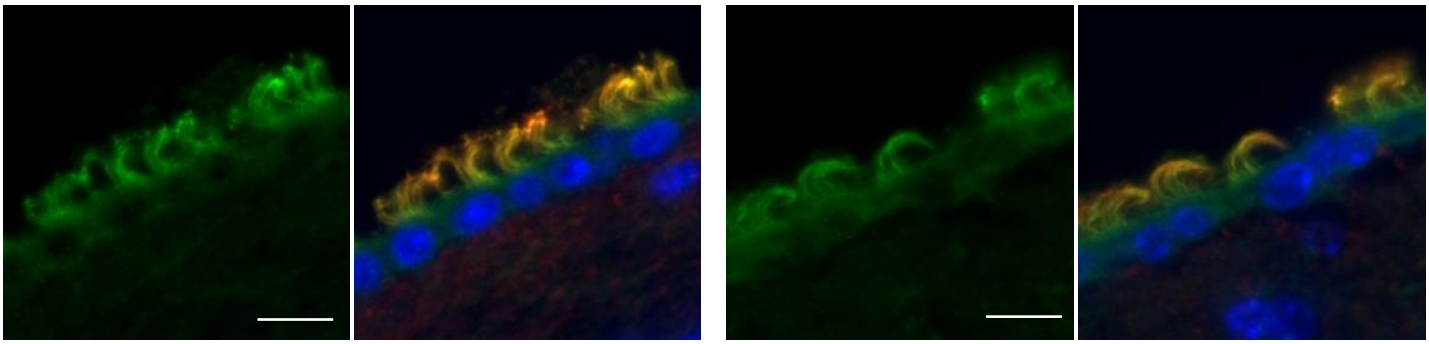

B

IFT88

+/+ -/-

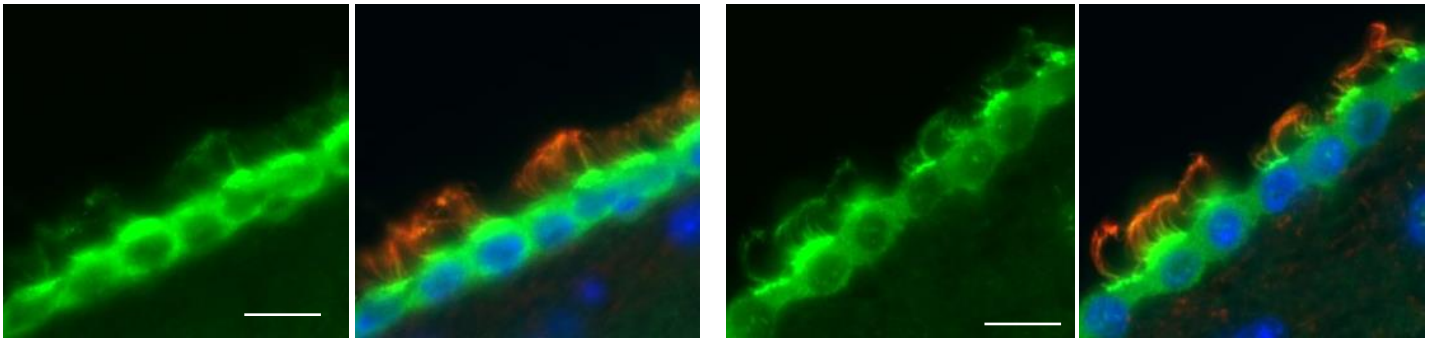

C

KIF3A

+/+ -/-

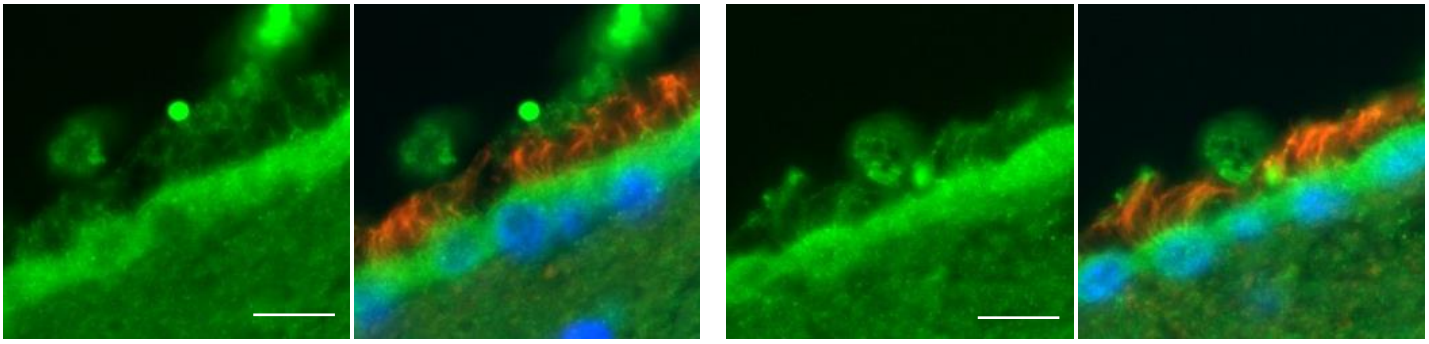

ac-α-tubulin **hoechst**

Supplement. 5